Hindawi Publishing Corporation
Advances in Meteorology
Volume 2012, Article ID 356265, 36 pages
doi:10.1155/2012/356265

Review Article

Lidar Measurements for Desert Dust Characterization: An Overview

L. Mona,[1] Z. Liu,[2] D. Müller,[2,3,4] A. Omar,[5] A. Papayannis,[6] G. Pappalardo,[1] N. Sugimoto,[7] and M. Vaughan[5]

[1] *Consiglio Nazionale delle Ricerche, Istituto di Metodologie per l'Analisi Ambientale (CNR-IMAA), C.da S. Loja, Potenza 85050 Tito Scalo, Italy*
[2] *Science Systems and ApplicationS Inc., c/o NASA Langley Research Center MS 475, Hampton, VA 23681, USA*
[3] *Leibniz Institute for Tropospheric Research (IfT), Permoserstraße 15, 04318 Leipzig, Germany*
[4] *Gwangju Institute of Science and Technology (GIST), 1 Cheomdan-Gwagiro, Buk-Gu, Gwangju 500-712, Republic of Korea*
[5] *NASA Langley Research Center, MS 475, Hampton, VA 23681, USA*
[6] *Laser Remote Sensing laboratory, Physics Department, National Technical University of Athens, 15780 Athens, Greece*
[7] *National Institute for Environmental Studies, 16-2 Onogawa, Tsukuba, Ibaraki 305-8506, Japan*

Correspondence should be addressed to L. Mona, mona@imaa.cnr.it

Received 15 February 2012; Revised 31 May 2012; Accepted 30 July 2012

Academic Editor: Aristides Bartzokas

We provide an overview of light detection and ranging (lidar) capability for describing and characterizing desert dust. This paper summarizes lidar techniques, observations, and fallouts of desert dust lidar measurements. The main objective is to provide the scientific community, including nonpractitioners of lidar observations with a reference paper on dust lidar measurements. In particular, it will fill the current gap of communication between research-oriented lidar community and potential desert dust data users, such as air quality monitoring agencies and aviation advisory centers. The current capability of the different lidar techniques for the characterization of aerosol in general and desert dust in particular is presented. Technical aspects and required assumptions of these techniques are discussed, providing readers with the pros and cons of each technique. Information about desert dust collected up to date using lidar techniques is reviewed. Lidar techniques for aerosol characterization have a maturity level appropriate for addressing air quality and transportation issues, as demonstrated by some first results reported in this paper.

1. Introduction

Dust is one of the main components of the atmospheric aerosol loading. It is estimated that dust particles account for about 75% of the global atmospheric aerosol load [1] with an annual rate of about 1-2 Tg of dust lofted into the atmosphere [2]. The main sources of dust are the large arid areas of the world: the African continent, especially the Sahara desert, the Arabian Peninsula, and the Asian continent (eastern areas) [3–8]. Dust particles that originated in these arid areas can be transported over long distances by strong winds and convective processes [9]. Saharan dust particles, for example, can cross the North Atlantic Ocean and reach the southeastern United States [7, 10].

Desert dust particles have many effects. They can impact climate, the precipitation cycle, and human health. Like all aerosol types, desert dust particles have direct and indirect effects on the radiation budget. The direct effect is the mechanism by which aerosols scatter and absorb short-wave and long-wave radiations and change the radiative balance of the Earth-atmosphere system. The latest report of the Intergovernmental Panel on Climate Change (IPCC) reports a range of the total direct radiative effect of dust from -0.56 to $+0.1\ \mathrm{W/m^2}$, with a medium-low level of scientific understanding [11]. Large uncertainties still remain about indirect effects of aerosols on radiation budget. The indirect effect is the mechanism by which aerosols modify clouds properties. Mineral dust particles can act as cloud condensation nuclei (CCN) and thereby determine the concentration of the initial droplets, albedo, precipitation formation, and lifetime of clouds [12–14]. All these parameters impact on the clouds ability to reflect and/or absorb radiation and thus alter

the Earth's radiation budget. In particular, mineral aerosols interact with liquid clouds by suppressing precipitation [15] and changing the ice content of clouds [16, 17]. A cause of the uncertainties on the influence of mineral aerosols on radiative forcing is the high variability both in time and space of dust concentration, shape, size distribution, refractive index, and vertical distribution [18]. The incomplete understanding of the processes responsible for the production, transport, physical and chemical evolution, and removal of mineral aerosols at various space and time scales is a further source of uncertainties of dust impact on the radiation budget [18, 19].

Dust particles present serious risks to the environment and human health for countries in dust source regions and surrounding areas [20]. Cardiovascular, respiratory, and lung diseases can be caused by the inhalation of submicron radii particles since these can be ingested deep in the human body [20–24]. Cases of eye infections and diseases such as meningitis and valley fever have been recorded during and after strong dust event in some regions [23, 25–27]. At larger distances from arid regions, elevated dust concentrations in air masses transported by the wind can exceed the limits established for air pollution by the air quality management authorities [28–30]. Such exceedances due to dust can lead to regulations limiting vehicular transportation and industrial activity. Studies have found evidence of adverse health effects of small particles with diameters less than 10 μm and 2.5 μm, referred to as PM_{10} and $PM_{2.5}$, respectively, during Saharan dust outbreaks [31–33] and suggest an association between respiratory mortality in the elderly and Saharan dust outbreaks [34].

In addition, sudden and severe dust storms can affect air and highway safety by reducing the visibility [20]. Desert dust can also cause significant problems in aviation by affecting aircraft engines and visibility [20, 35]. Such phenomena lead to rerouting aircraft due to poor visibility, disturbances in airport operations due to delays and massive cancellation of scheduled flights, and mechanical problems such as erosion and corrosion of aircraft engines.

Because of the manifold impacts of dust, there is a high interest in coordinating both observations and efforts for dust investigations at the international level. In 2007, the World Meteorological Organization (WMO) established the Sand and Dust Storm Warning Advisory and Assessment System (SDS-WAS) (http://www.wmo.int/pages/prog/arep/wwrp/new/Sand_and_Dust_Storm.html) in response to the desire of 40 WMO member countries to improve capabilities for more reliable sand and dust storm forecasts [20]. SDS-WAS is a federation of partners organized around two regional nodes: the Northern Africa-Middle East-Europe Node (hosted by Spain) and the Asian Node (hosted by China). The SDS-WAS integrates research and user communities (e.g., medical, aeronautical, and agricultural users). The SDS-WAS's mission is to achieve comprehensive, coordinated, and sustained observations and modeling capabilities of sand and dust storms in order to improve their monitoring, to increase the understanding of the dust processes, and to enhance dust prediction capabilities. In particular, real-time data from atmospheric dust models may strongly contribute to risk reduction of different impacts. Because of this reason, SDS-WAS main objective is to enhance operational dust models through assessment/validation and assimilation of observational data.

From the observational point of view, satellite observations by passive sensors such as the Moderate Resolution Imaging Spectroradiometer (MODIS), the Spinning Enhanced Visible Infrared Imager (SEVIRI), the Multiangle Imaging Spectrometer (MISR), the Ozone Monitoring Instrument (OMI), and, during the past, the Total Ozone Mapping Spectrometer (TOMS) [7, 36–43] are very important tools for tracking dust plumes and identifying dust sources. The advanced retrieval algorithms developed for these sensors now provide highly reliable information about aerosol optical depth (AOD) and its fine/coarse mode fraction (e.g., [44]). Observations from satellite-borne passive sensors extend over large horizontal distances, facilitating the identification of dust occurrence and transport. Though some passive sensors are capable of identifying multiple layers in the atmospheric column, lidar (light detection and ranging) provides the highest vertical resolution (on the order of tens of meters) for the investigation of interaction with clouds, layering, and a number of other related application possibilities. In this context, lidar technique has the unique capability of providing information about the vertical distribution of the particles required to address these topics. Lidar is an active remote sensing technique based on the principle that information from the atmospheric structure and constituents can be obtained from how the laser light transmitted into the atmosphere interacts with the atmosphere and is backscattered by various targets (gases, particles, and cloud droplets) before being collected by an appropriately designed optical receiving system. The rapid evolution of laser and detector technologies was the main driver of the quick progress in lidar techniques starting from the first lidar application for atmospheric studies in 1963 when scattering layers between 69 and 140 km were detected [45]. In the beginning, lidar applications for aerosol were mainly limited to research activities with the development of the first ground-based aerosol lidars (e.g., [46–50]) and related inversion procedures (e.g., [46, 47, 51–57]). The first lidar observations of dust from space were recorded during the LITE experiment [58, 59] and, after that, by the GLAS satellite [60], making clear the promising capability of lidar for dust observations from space. Nowadays lidars have attained a high degree of reliability and have been used by regional networks to produce long-term, self-consistent, and well-calibrated measurements of aerosol properties. These include the European Aerosol Research Lidar Network (EARLINET) (http://www.earlinet.org/) [61], a federation of several European research groups established to produce a self-consistent aerosol climatology; the Asian Dust Network (AD-Net) (http://www-lidar.nies.go.jp/AsiaNet/),established in 1998 to obtain 4D perspectives of Asian dust transportation using distributed lidar sites in Asian countries [62]; the Micropulse Lidar Network (MPL-Net) (http://mplnet.gsfc.nasa.gov/), a federated network of Micro Pulse Lidar (MPL) systems designed to measure aerosol and cloud vertical structure [63]. All these networks participate in the Global Atmosphere Watch (GAW) Aerosol Lidar Observation

Network (GALION) promoted by the WMO with the main long-term objective of providing the vertical component of aerosol distributions through advanced laser remote sensing in a network of ground-based stations [64].

Besides these research-oriented networks, there are a large number of ceilometers distributed worldwide. Ceilometers (often called low-power lidars) are very robust systems for continuous operation that can provide useful information about the aerosol layers. Particularly interesting in this field is the over 40-networked ceilometers of the German Weather Service (DWD) [65]. The widely distributed ceilometers could also contribute to the characterization of aerosol horizontal distribution.

Global information on vertical profiles of both aerosol and clouds optical properties and layering is provided by CALIOP (Cloud-Aerosol lidar with Orthogonal Polarization), the lidar on board CALIPSO (Cloud-Aerosol Lidar and Infrared Pathfinder Satellite Observation) satellite, which has been making measurements nearly continuously since June 2006 [66].

The potential applications of lidar techniques to measure desert dust are numerous. The intrusion into the Planetary Boundary Layer (PBL) of desert dust and mixing processes of dust with other aerosol types can be investigated in detail using the vertical profiling capability of lidars (e.g., [67–75]). Long-range transport of dust can be monitored and tracked by ground-based lidar networks or spaceborne lidars [76–81]. Lidar measurements in combination with other techniques are ideal to investigate certain aspects of atmospheric composition, transport, and deposition of dust. Furthermore, lidar measurements can be used to investigate both aerosol and cloud properties (e.g., [17, 47, 60, 82–89]): the profiling capability permits the simultaneous detection of aerosol and cloud layers. This aspect in conjunction with the high temporal resolution typical of lidars is optimal for aerosol/cloud interaction studies, particularly for investigating cloud formation processes as a function of aerosol content. Therefore, the aerosol indirect, and in particular secondary indirect, forcing effect on the radiation budget can be studied by taking advantage of the lidar profiling capability [90, 91]. The lidar/radar synergistic approach is a novel and promising research field in this context [92].

Lidar techniques can be an important tool not only for dust investigation and study but also for practical applications concerning, for example, air quality and transportation (e.g., [20, 28, 30, 35]). Nevertheless, lidar capability and potential in dust monitoring and investigation are not well known to the wider community of non-practitioners of lidar observations and data analyses. This paper aims to provide the reader with a useful reference in which lidar capabilities and results for dust investigation are presented to the wider user community beyond lidar specialists. The different lidar techniques for dust investigation are described in Section 2. This paper documents lidar capabilities to measure temporally and vertically resolved aerosol properties and attributes such as aerosol layering and typing, aerosol sources and seasonal variation, long-range transport, and intrusion into the boundary layer. These capabilities are shown through the description of the value added by lidars during the measurement campaigns (Section 3). Dust information provided by ground-based lidars, networks, and satellite-borne lidars is reported focusing on the most advanced observations currently available (Sections 4 and 5). In particular, coordinated measurements performed within networks permit the investigation of differences due to the dust transport through the network. Climatological analyses are possible thanks to long-term measurements as those available within well-established networks and satellite-based measurements. First examples of evaluation of models and assimilation in dust models of lidar systematic observations of dust are reported in Section 6. In Section 7, we review potential applications of lidar dust measurements relevant to air quality and transportation. Finally, concluding remarks and future perspectives are given in Section 8.

2. Lidar Techniques

First developed in 1963 [45], lidar techniques for atmospheric studies are nowadays recognized as the most powerful tools for investigating the vertical structure and composition of the atmosphere at high resolution. Lidar techniques permit range-resolved investigation of atmospheric water vapour [48, 93, 94], temperature [95, 96], wind [97, 98], ozone [96], pollutants [99], hydrocarbons [100], aerosols [47, 49, 53, 66], and clouds [47, 66, 101] with important applications to air quality assessment (e.g., [30]), climate change [11], and meteorological fields [102]. Lidar techniques provide vertical profiles of aerosol optical properties with high resolution both in time and space and are very effective for aerosol source identification [75, 85, 103–105] and detection of the intrusion of long-range-transported aerosol into the Planetary Boundary Layer (PBL) (e.g., [74, 75]).

It is worth noting that there are different techniques for the investigation of aerosol properties using lidar from the easiest and widely distributed simple elastic backscatter lidar, to complex and advanced multiwavelength Raman lidar and High Spectral Resolution Lidar (HSRL). In the following section, the common scheme and the differences among the lidar techniques most widely applied for aerosol investigation are briefly described. A complete review of lidar techniques and their applications is reported in [106]. Here, after a short reference to basic single-scattering lidar equation, attention is focused on the diversity of quantitative data retrieved from the various techniques.

The basic equation describing the lidar detected signal $P(\lambda, \lambda_L, R)$ is

$$P(\lambda,\lambda_L,R) = P_L \frac{c\tau_d}{2}\frac{A_0}{R^2}\xi(\lambda)\beta(\lambda,\lambda_L,R) \times \exp\left(-\int_0^R \alpha(\lambda,R')dR'\right) \cdot \exp\left(-\int_0^R \alpha(\lambda_L,R')dR'\right), \quad (1)$$

consisting of two main parts. The first part consists of the following constants and instrumental factors:

(i) P_L is the average power of a single laser pulse;

(ii) c is the light speed, τ_d is the temporal pulse length, so that $c\tau_d/2$ is the length of the volume from which backscattered light is received at an instant time;

(iii) A_0/R^2 is the solid angle of perception of the lidar for light scattered at distance R from the detector, with A_0 denoting the telescope area;

(iv) $\xi(\lambda)$ represents the overall efficiency of the system at the wavelength λ.

All information regarding the state of the atmosphere is instead embedded into the last three factors of (1). In particular:

(i) $\beta(\lambda, \lambda_L, R)$ is the backscatter coefficient and represents the light scattered at the λ wavelength by the atmosphere at a distance R from the receiver when a laser pulse at λ_L wavelength is injected into the atmosphere itself;

(ii) the exponential term. $\exp(-\int_0^R \alpha(\lambda, R')dR')$ is the transmissivity between the detector and the distance R at the wavelength λ. In this expression $\alpha(\lambda, R')$ is the extinction coefficient at wavelength λ and indicates the loss or attenuation of light at wavelength λ at distance R'.

The product $\beta(\lambda, \lambda_L, R)\exp(-\int_0^R \alpha(\lambda, R')dR') \cdot \exp(-\int_0^R \alpha(\lambda_L, R')dR')$ is referred to as the attenuated backscatter and is directly measured by backscatter lidars.

This is the basic equation for all the lidar techniques. Particular variations of it are applied for each one of the specific techniques discussed in the following.

The basic product of aerosol lidar technique is the aerosol backscatter, β. The level of retrieval accuracy of β depends on the lidar technique used. Figure 1 shows the growing complexity of lidar techniques and, correspondingly, the increasing number of direct products.

The simplest lidar for aerosol study is the elastic backscatter lidar. Its simplicity and relatively low cost makes it the most common ground-based lidar worldwide. On the other hand, CALIOP, the first satellite-borne lidar specifically designed for aerosol and cloud studies, is an elastic backscatter lidar and has been continuously providing aerosol extinction, backscatter, and depolarization ratio profiles nearly continuously since June 2006 around the globe. As a result, the most common profile measurements for aerosol studies are presently provided by elastic backscatter lidars. These are shown at the base of the pyramidal structure on the left of Figure 1. The shadow of the base of this structure is the ceilometer, a low power elastic backscatter lidar device that uses a laser source to determine the height of the base of clouds, or the so-called "cloud ceiling." Ceilometers can also be used to measure the aerosol layer heights in the atmosphere, as briefly discussed below.

In the simple elastic configuration, (1) can be solved using retrieval methods (e.g., [51–54, 107]), through two main assumptions: the backscatter profile needs to be calibrated, and a linear relationship between aerosol extinction and backscatter is assumed. For the backscatter calibration, typically it is calibrated to zero value in an altitude range where the aerosol content can be neglected. Systematic error associated with this assumption depends on the aerosol load and can reach 60% in the free troposphere [108]. Typically, one assumes certain extinction to backscatter ratio, hereafter lidar ratio (S), based on values reported in the literature to enable retrieval since (1) is underdetermined. Lidar ratio is an important optical parameter in aerosol characterization, because it depends on intensive aerosol properties such as chemical composition, size distribution of the particles, and particle shape [109–111]. A constant, altitude independent, value is often assumed. This assumption results in an uncertainty in the primary product of this technique, the aerosol backscatter coefficient profiles. This uncertainty can reach up to 150% [108] and can be reduced by constraining the derived total column aerosol optical depth (AOD) to the values obtained by independent sensors such as sunphotometers (e.g., [112]). However, it should be noted that lidar profiles typically do not reach the ground because of the incomplete overlap between the field of view of lidar telescope and the laser beam in the lowest altitude ranges. Even if some methods exist for evaluating the overlap correction function aspect (e.g., [113, 114]), an assumption about the lowest altitudes of the atmosphere is needed for the AOD evaluation from lidar profiles. The uncertainty resulting from these assumptions is strongly dependent on the overlap correction of each lidar system and on the atmospheric conditions. In this regard, a low overlap and a stable well-mixed PBL conditions reduce the error on lidar evaluated AOD [113].

In any case, different values of lidar ratio are expected in layers of different aerosol types (e.g., [109, 111, 115, 116]). In some cases, the lidar ratios can be different for the same kind of aerosol if the aerosol and/or atmospheric properties (e.g., dimension, refractive index, shape, chemical composition, and humidity content) vary within layers [115]. Besides first attempts to improve the backscatter retrieval through integration with sunphotometer measurements (e.g., [117]), the most common procedure applied, for example, in the CALIOP retrieval, is to associate a certain lidar ratio value with each aerosol layer after the aerosol type has been identified. Simulation and theoretical studies provide some reference values for different aerosol types also as a function of relative humidity (e.g., [111, 115, 116, 118]). So far, there have been very few attempts to derive aerosol-type-dependent lidar parameters in a systematic way. Cattrall et al. [119] have published lidar parameters of five key aerosol types (marine, urban, biomass-burning, dust, and Southeast Asian aerosol) derived from AERONET sunphotometer measurements. However, the reliability of these values is limited because the sunphotometer cannot measure the particle backscatter coefficient, but estimates it from products of inversions. This leads to not negligible uncertainty especially in cases of nonspherical particles, as large dust particles. In addition, the AERONET climatological study is based on column measurements and therefore assumes that a single

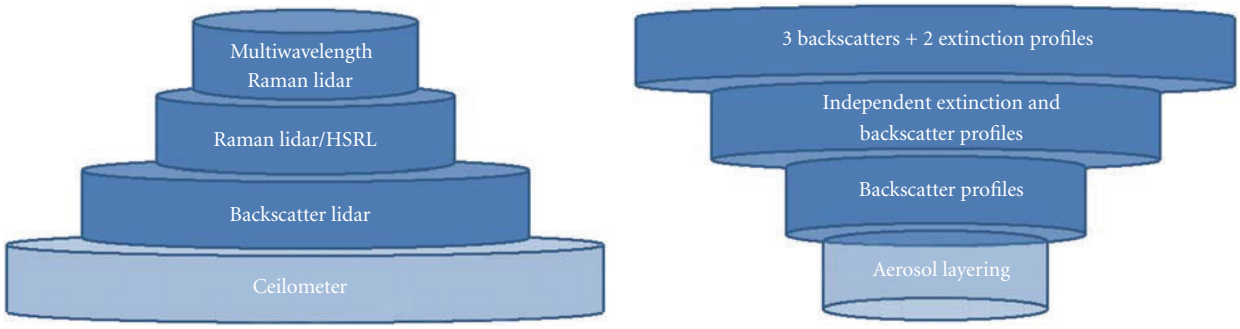

Figure 1: Aerosol lidar techniques pyramidal diagrams: complexity/distribution (a) and corresponding top level products (b).

type of aerosol is present in the column, which in most cases is unlikely. Furthermore, the study assumes that a single aerosol species dominates the atmospheric column based on geographic location, time of year, and seasonal events. All these assumptions lead to significant yet unquantified uncertainties in the aerosol lidar ratios reported.

Directly measured S values, as those obtained by using more complex lidar techniques described below, are more suitable as reference values for the different aerosol types and subtypes (e.g., [120]). However, direct measurements of S show that this parameter is highly variable for the same type of aerosol and even considering just one measurement site (e.g., [79, 121–123]). This means that reasonable assumptions should be made about the S profile to reduce the error in the backscatter profile. In the end, the uncertainty affecting backscatter cannot be disregarded as it can reach 50% for a difference in S of 20 sr depending on the aerosol optical depth [108]. Because the aerosol extinction varies with the wavelenght as $\lambda^{-\delta}$ where δ is typically positive, the backscatter is more sensitive to S variation in the ultraviolet wavelengths (e.g., 355 nm) than for longer wavelengths.

Aerosol extinction profiles retrieved by simple elastic backscatter lidars are often reported in literature and historically Klett's method provides solution in terms of extinction [53]. However, it is practically hard to retrieve the extinction profiles through this method [51, 53, 64] and typical extinction errors can be a factor five over backscatter errors [64]. Therefore, when Klett's (or similar) method is used for inverting lidar equation, the method is used in the backscatter form. On the base of these considerations, the aerosol extinction coefficient is not reported as a measured parameter for the simple backscatter lidar techniques in Table 1.

Ceilometers that often referred to as low-power backscatter lidars are shown as the shadow base of the lidar technique pyramid reported in Figure 1. Originally designed for cloud top and base identification, ceilometers proved to be an efficient instrument for identifying and following long-range transport of volcanic emissions during the Eyjafjallajökull volcanic eruption in 2010 [124]. The automatic and 24-hour 7-day operation of these instruments together with the large number of ceilometers available worldwide makes them suitable candidates for an operational low-cost monitoring system. Little has been done until now on the quantitative evaluation and assessment of ceilometer efficiency in aerosol layer detection and characterization [65, 125–128]. Since ceilometers are based on the principle of a simple backscatter lidar, the same discussion of the aerosol backscatter coefficient retrieval applies to ceilometers where the low signal-to-noise ratio poses additional challenges in the application of the retrieval techniques. In particular, the calibration of infrared signals is often not possible because of the low signal-to-noise ratio (SNR) and in some cases thick aerosol layers in the low atmosphere attenuate the low-intensity ceilometers signal in such a way that upper layers are not detectable [126]. Therefore, the standard product of ceilometers suitable for aerosol studies is the time-altitude evolution plot of normalized range-corrected (background subtracted) signals. These plots, available for each kind of lidar system, provide a snapshot of the aerosol vertical distribution, and albeit, at a qualitative level, provide valuable information not available from passive sensors.

The only elastic lidar method that makes it possible to obtain extinction profiles from elastically scattered signals without the assumption on lidar ratio profile is the method proposed by Kano [56] and Hamilton [57] for the inversion of data obtained with scanning lidar.

For multiangle lidar, (1) slightly changes: the β term is related to the specific observation angle used in each scan and the transmissivity term is angle dependent. With observations performed at different angles, extinction profile can be retrieved assuming that the backscatter term is invariant in horizontal layers. Unfortunately, multiangle methods can yield poor inversion results (e.g., [50]), mainly because of the homogeneity assumption [129]. For this reason, multiangle methods are rarely used in lidar measurements. The recently developed data-processing technique proposed by Kovalev et al. [130] is highly innovative in this context: this technique rejects the signals that do not obey the condition of atmospheric homogeneity or have significant systematic distortions. The new technique enables discrimination of thin-stratified layers [130].

Two types of lidar techniques, namely, Raman lidar and HSRL, are available for independent retrieval of the extinction profile. Both of these directly measure the aerosol extinction profile, which can be inserted in (1) to calculate aerosol backscatter coefficient sans assumptions.

Table 1: Products for each specific lidar technique. Quantities obtained by directly measured parameters, (S is the lidar ratio, Å (α) is the Angstrom extinction related exponent, and Å (β) is the Angstrom backscatter related exponent), are also reported. Finally, critical assumptions/points for each technique are reported too.

Lidar techniques	Aerosol layering	Extensive properties	Intensive properties	Critical aspects	Systematic errors
Ceilometer	- PBL top - FT layers* (top, base, center of mass)	Aerosol backscatter*	n.a.	- S assumption - Calibration often not possible	*Calibration*: up to 60% in free troposphere (larger at longer λ) *S assumption*: also 150% in the free troposphere (larger at shorter λ)
Backscatter lidar	- PBL top - FT layers (top, base, center of mass)	Aerosol backscatter	$S^{\dagger}$	S assumption	*Calibration*: up to 60% in free troposphere (larger at longer λ) *S assumption*: also 150% in the free troposphere (larger at shorter λ)
Raman lidar	- PBL top - FT layers (top, base, center of mass)	- Aerosol backscatter - Aerosol extinction	S	Low SNR in daytime	*Density*: <15% for backscatter <5% for extinction *Angstrom assumption* <1% for backscatter <4% for extinction
HSRL	- PBL top - FT layers (top, base, center of mass)	- Aerosol backscatter - Aerosol extinction	S	Instrumental complexity	*Calibration*: about 2.5% (backscatter and extinction) *Density* <5% for extinction
Multi-wavelength HSRL/Raman lidar	- PBL top - FT layers (top, base, center of mass)	- Aerosol backscatter at 3 wavelengths - Aerosol extinction at 2 wavelengths	1 S 1 Å (ext) 2 Å (back)	Low SNR in daytime (Raman) Instrumental complexity (HSRL)	*Typical total systematic errors*: <5% for backscatter <10% for extinction

The symbol † indicates that S can be retrieved for specific cases with clean air below and above identified intense aerosol layer. Depolarization capability could be added to each one of these techniques resulting in the additional aerosol linear depolarization ratio measurement capability. The symbol * denotes products that could be not available because of the low signal-to-noise ratio.

In the combined elastic/Raman lidar, the inelastically (Raman) backscattered lidar signal is measured besides the elastically backscattered one [46, 47]. In particular, the Raman signal due to molecules whose density in the atmosphere is well known, such as nitrogen or oxygen, permits the determination of the aerosol extinction profile. In these cases, the backscatter term in (1) is known and the only unknown is the extinction profile. The retrieval of aerosol extinction coefficient requires an assumption about the wavelength dependence of the aerosol extinction (referred to as the Ångström exponent), because (1) contains in this case a transmissivity term at laser wavelength and one at wavelength corresponding to the Raman shift. Whiteman [131] showed that the differential transmissivity varies by about 4% for an Ångström exponent varying between 0.8 and 1.2 for an optical depth of 1.0. The systematic error due to the assumption of the extinction dependence on wavelength is lower than 4% for Ångström exponent variation of 100% and than 1% for Ångström exponent varying between 0 and 1, for aerosol extinction and backscatter retrieval, respectively [46]. This systematic error can be further reduced if Angstrom exponent measurements are available from independent source (e.g., Sun-photometer). Another source of possible systematic error is the assumption of the atmospheric density profile in (1). However, the density error is less than 5% for both aerosol extinction and backscatter profiles when standard atmosphere profiles are used [46]. This error can be reduced using collocated simultaneous radiosounding when available.

Elastic/Raman lidars were rare until the 1990s when the advances in both detector and interferential filter devices allowed for a progressive spread of this kind of systems for aerosol characterization. The low signal-to-noise ratio (SNR) compared to elastically backscattered signal typically limited the application of elastic/Raman technique to nighttime conditions in the past. Nowadays, Raman lidar measurements are possible in daytime conditions with appropriate temporal and spatial signal averaging [132].

The combined elastic/Raman lidar technique has the great advantage of allowing the determination of aerosol extinction profiles without any significant assumptions and consequently the determination of the aerosol backscatter profile with uncertainty significantly lower than the simple backscatter lidar [47]. Moreover, the independent measurement of aerosol extinction and backscatter profiles permits the direct measurement of lidar ratio profile. Measurements of this parameter are important because it is required for the retrieval of optical properties from the aforementioned widely used standard elastic-backscatter lidar. In addition, lidar ratio is a very important parameter for the characterization and typing of aerosols. This kind of measurements with the support of transport models permits a detailed investigation of aerosol typing and mixing processes (e.g., [85, 121, 133, 134]).

The principle of the High Spectral Resolution Lidar is, as for Raman technique, to use two independent lidar equations instead of the single one of backscatter lidars [55]. In this case, the difference in the Doppler frequency shifts produced by photons scattered by molecules (random motion) and by particulate (motion determined by wind and turbulence) is utilized. The difference in velocity of these two classes of scattering particles produces significantly different Doppler shifts for molecules and particles. Particles in the atmosphere generate a narrow spike near the frequency transmitted by the laser. On the contrary, atmospheric molecules produce a much broader distribution.

HSRL utilizes very narrow bandwidth filters to select signal backscattered from molecules. Particular attention has to be paid to the stability and purity of the laser transmitting frequency. In this way, two distinct equations of analogous to (1) are obtained: one for the molecular backscatter and the other for the particulate backscatter. In both, the integral factor contains the aerosol and molecular contributions to the extinction. Therefore, as for the elastic/Raman technique, the availability of two equations for two unknowns (i.e., aerosol extinction and backscatter coefficient) permits the independent measurements of these parameters and consequently of the lidar ratio. The systematic error in the aerosol backscatter coefficient is derived from the internal calibration and is estimated to be typically less than 2.5% [135]. As in the Raman lidar technique, the aerosol extinction coefficient retrieval needs for assumption about the air density profile. As such, the systematic error in extinction associated with uncertainties in the density profile is the same found for Raman lidar systems [135].

In comparison with the Raman technique, the HSRL has the advantage of providing molecular signal with an SNR much higher than Raman signal SNR. HSRL is therefore more suitable for both daytime and airborne/satellite-borne applications. On the other hand, the HSRL technique required high stability and a small line width of transmitted laser frequency making HSRL more difficult to implement than Raman lidars. The Raman lidar technique is more often utilized by ground-based lidars resulting in a more extensive geographical distribution of Raman lidar sites at least in the Northern Hemisphere. The HSRL is typically implemented on airborne platforms for measurement campaigns and will be the lidar technique implemented both on ESA the Atmospheric Dynamics Mission (ADM-Aeolus) [98] and on the Earth Clouds Aerosols and Radiation Explorer (EarthCARE) mission of ESA and JAXA [136], to be launched on 2013 and 2015, respectively.

The most advanced state-of-the-art ground-based lidars make use of a multiwavelength approach. In a typical configuration, three laser beams are transmitted into the atmosphere and the corresponding three elastically backscattered signals are detected along with two Raman-shifted signals due to atmospheric nitrogen. These advanced systems, hereafter multiwavelength Raman system, provide a suitable dataset of aerosol optical properties profiles (3 backscatter + 2 extinction, 3 + 2 hereafter) for the aerosol typing (e.g., [75, 121]) and the retrieval of aerosol microphysical optical properties by the application of specific inversion algorithms [137–139]. Multiwavelength Raman aerosol lidar techniques have been demonstrated to have the unique ability of providing range-resolved aerosol microphysical properties, as effective radius and complex refractive index (e.g., [140]). Finally, this kind of measurements combined with

sunphotometer observations could permit the determination of the aerosol mass concentration profile and of its fine and course components [141, 142].

Information about the shape of the particles is provided by measurements of the depolarization of the light into the atmosphere. The depolarization measurement in lidar applications is based on the transmission into the atmosphere of a linearly polarized laser pulse and the detection of components of backscattered light polarized perpendicular and parallel to the direction of the transmitted laser beam. Little or no linear depolarization is expected for small, spherical particles, while large linear depolarization ratio values are found for irregularly shaped aerosols and ice crystals with values depending on the size, shape, and orientation of the particles [101]. The linear particle depolarization ratio measurement is possible when polarization channels are also implemented, in the various lidar systems described above. The linear particle depolarization ratio δ is defined as the ratio of cross-polarized component of the backscatter from particles to the parallel component [143]. This adds a further intensive property (i.e., independent on the quantity of aerosol particles), which has the potential of aiding aerosol typing. At the present, lidar systems in general only employ one wavelength to infer the linear particle depolarization ratio and this capability is implemented on simple one-wavelength backscatter lidars (economic solution) or on multiwavelength Raman lidar (expensive solution). The multiwavelength Raman lidar systems equipped with depolarization channel (so-called $3 + 2 + \delta$ lidar systems) are nowadays the most advanced systems providing the most extended dataset of aerosol optical parameters for aerosol characterization.

Recently, a new type of lidar has been developed, in which Raman return signals from silicon dioxide can be used as a tracer of mineral dust. Showing the general applicability of using such Raman return signals for inferring the mineral dust concentration in East Asian dust plumes [144], a major advance was made by combining this technique with a $3+2+\delta$ lidar system [145, 146].

Table 1 reports the measurable quantities for the lidar technique described above. In addition, an indication of the systematic errors related to each one of the retrieval techniques is reported. Systematic errors are errors related to the physical assumptions needed for the retrieval procedures; therefore, they do not depend on the specifics of the lidar system. These systematic errors provide an indication of the intrinsic limits of each lidar technique. A common product of all lidar techniques is the profiling capability, that is, the aerosol layering. The provision of detailed aerosol layering is limited by the signal-to-noise ratio that in low-power lidars such as ceilometers does not always permit the aerosol layering in the free troposphere [126]. Base, top, and thickness of the aerosol layers can be determined with the high range resolution typical of the lidar techniques using different algorithms (e.g., [128, 147–149]). Once top and base of desert dust layer are identified, the center of mass of the aerosol layer can be also estimated from lidar profiles [123]. Information about the aerosol layer center of mass is useful because the dynamics of the whole layer can be discernible at this location. Under the hypotheses of a homogenous aerosol layer with respect to aerosol microphysical properties, the center of mass can be estimated as the mean altitude of the identified desert dust layer weighted by the altitude-dependent aerosol backscatter coefficient.

The top of the PBL can be determined with lidar, as long as the overlap of telescope's field of view and laser beam permits it [128, 147].

The common aerosol optical property to all techniques is the aerosol backscatter coefficient that can be retrieved with all techniques, with some limitations for ceilometers related to the SNR and calibration. Raman and HSRL techniques permit the addition of extinction as an extensive aerosol property and lidar ratio as intensive. Here, intensive refers to a property that is independent from the amount of aerosol. Adding channels, in elastic or Raman lidar systems, increases the number of aerosol optical properties that can be retrieved. It increases the number of aerosol extinction and backscatter profiles, and more wavelengths allow measurement of Ångström extinction and backscatter exponents, and S in ultraviolet and visible wavelengths. In the particular situation of an aerosol layer surrounded by clean air layers below and above it (as stratospheric layers), the lidar ratio can be determined by the simple elastic backscatter lidar with the assumption of a homogenous aerosol layer in terms of microphysical properties (e.g., [150]).

For each technique reported in Table 1, additional channels for the detection of depolarized and/or unpolarized backscattered signals permit to retrieve the particle linear depolarization ratio profile.

Starting from this dataset of optical properties and geometrical layering, columnar quantities, such as AOD, can be retrieved. This also allows the PBL and free troposphere contribution to be evaluated. Each aerosol layer can be characterized in terms of available optical extensive and intensive properties. These quantities are the basis for the determination of aerosol microphysical properties using appropriate numerical methods.

In that regard significant progress has just recently been made. Veselovskii et al. [151] used a modified data inversion algorithm [152] for the retrieval of dust microphysical parameters (particle size distribution from which effective radius can be inferred, and the complex refractive index) from a set of lidar optical data that consisted of backscatter coefficients at 3 wavelengths, extinction coefficients at 2 wavelengths, and the depolarization ratio at one wavelength. The data set described a mixed Saharan dust/continental haze plume observed over Southwest Germany in summer 2007. The authors show that a retrieval of the aforementioned microphysical parameters is possible on a vertically resolved scale. The authors also showed the utility of depolarization ratio in the retrievals.

One drawback of the study by Veselovskii et al. [151] is that only a limited optical data set of a complicated aerosol situation (mixture of dust with a second aerosol type) was available. The large dataset collected during the SAMUM campaigns (see Section 3) provides instead the opportunity to investigate complex aerosol situations. A set of optical data of high quality (high signal-to-noise ratio) was collected

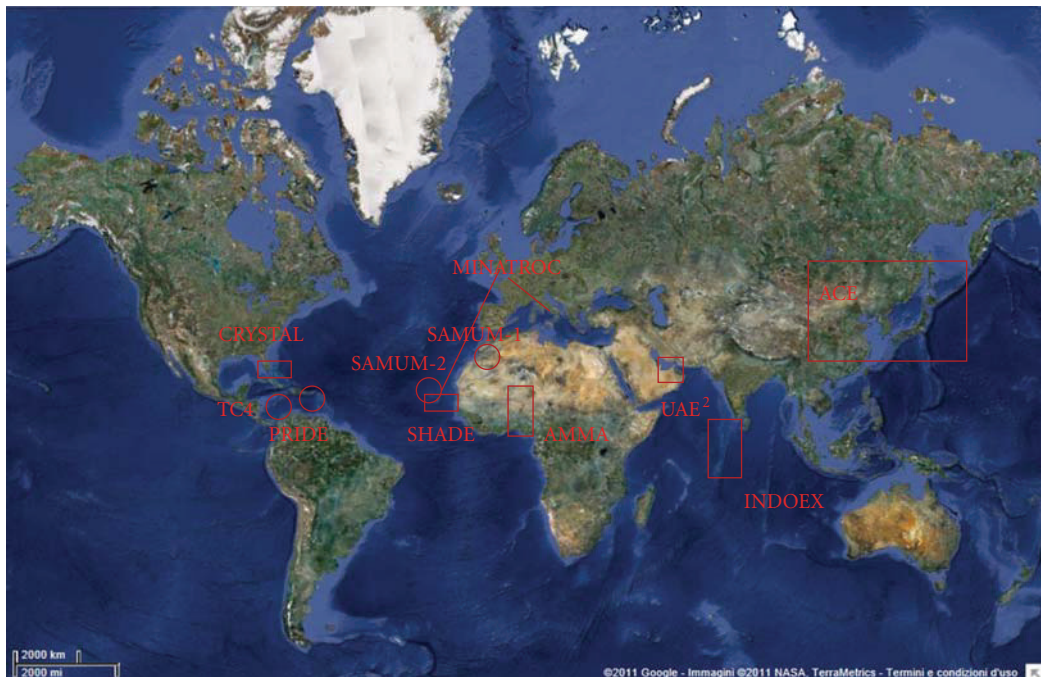

Figure 2: Location of the special measurements campaigns reported in Table 2.

with three ground-based Raman and airborne high-spectral-resolution lidar systems under various conditions of pure mineral dust (Morocco) [153] and mixtures of mineral dust, marine, and biomass burning aerosols at Cape Verde [154]. These studies produced a dataset of particle backscatter and extinction coefficients and lidar ratios at visible (532 nm) and ultraviolet wavelengths (355 nm) and profiles of Ångström exponents. In addition, profiles of depolarization ratios for four wavelengths (355, 532, 710, and 1064 nm) were also determined [143, 155]. Several case studies of pure dust and mixed dust/biomass-burning plumes were used for inferring dust microphysical properties [156]. Lidar data inversion results for the first time were validated using airborne observations of particle size distributions of dust. The complex refractive index was inferred from mineralogical analysis of particles collected aboard the aircraft. These data are critical for the validation of the complex refractive index inferred from the inversion of the multiwavelength lidar data.

Figure 1 and Table 1 show that increasing the complexity of the lidar technique could in principle reduce uncertainty on lidar data products and increase the number of available aerosol properties. However, statistical errors are not considered in this discussion, because they strictly depend on the specific design of each individual lidar system. Besides the used lidar technique, the practical implementation of the lidar system and data processing are fundamental factors driving the quality of the lidar data products. This is the reason why a rigorous check of the instrument and proper data processing and analysis techniques are fundamental for the investigation of dust at global scale. A globally coordinated action about this issue is foreseen by the implementation plan of GALION, the global lidar network promoted by the WMO [64].

3. Desert Dust Measurement Campaigns

Several international coordinated experimental campaigns for dust (and aerosol) particle characterization using mainly ground-based and airborne lidar systems have been conducted so far, at the regional or continental level in or near dominant source regions of mineral dust particles: North Africa (Sahara), Arabian Peninsula, Central Asia, China (Gobi), Australia, North America, and South Africa. In the following the most important measurement campaigns for dust characterization (Table 2 and Figure 2) are briefly described focusing on the value added by lidar observations.

Some systematic lidar measurements were performed during the Mediterranean Dust Experiment (MEDUSE) in two sites: Southern France (Observatoire de Haute Provence) and Northern Greece (city of Thessaloniki) during 1996-1997 [157]. These measurements were dedicated to the characterization of the vertical structure of Saharan dust export to the Mediterranean area, confined between 1.5 and 5 km height. In two cases, AOD of the order of 0.3-0.4 (at 532 nm) derived from lidar and sunphotometer measurements was reported.

During the Indian Ocean Experiment (INDOEX) lidar measurements were made on the Indian subcontinent and at locations in the Indian Ocean between February 15 and March 25, 1999 [158], and during the three follow-up campaigns in July/October 1999 and March 2000. Müller et al. [69] presented for the first time a comprehensive data set of vertically resolved microphysical particle properties: effective particle radii were $0.20 \pm 0.08\,\mu$m mostly from pollution plumes above 1 km height, the range of single-scattering albedo was between 0.75 and 1.00 at 532 nm, and the aerosol volume concentrations ranged from 6 to $44\,\mu m^3\,cm^{-3}$.

Table 2: Synthesis of the most important measurement campaigns for dust characterization involving lidar measurements.

Measurement campaign	Location	Period	Main references	Instruments	Lidar added value
INDOEX (Indian Ocean Experiment) http://www-indoex.ucsd.edu/	Indian subcontinent and Indian Ocean (8°N–8°S, 70°E–80°E)	January–March 1999	[69, 158]	*Ground-based:* - Gas samplers/Proton Transfer Reaction; Mass Spectrometer (PTR-MS)/Atmospheric Pressure Chemical Ionization Mass Spectrometer (AP-CIMS) - micro pulse lidar/multi-wavelength lidar	First vertical resolved microphysical properties: $r_{\text{eff}} = 0.20 \pm 0.08\,\mu$m SSA at 532 nm = 1–0.25 C_v = 6–44 μm^2/cm^3
PRIDE (Puerto Rico Dust Experiment) http://modis-atmos.gsfc.nasa.gov/PRIDE	Puerto Rico (18.21°N–65.60°W)	28 June–24 July 2000	[67, 159–161]	*Ground-based* - surface station/2 AERONET Sun-photometers/MICROTOPS sunphotometer - micro pulse lidar *Airborne:* - AATS-6 Sun-photometer/radiometers /2optical counters *Research vessel:* - in situ sensors	Highly variable layering: Dust up to 5 km Dust intrusion in the marine boundary layer
SHADE (Saharan Dust Experiment)	Sal Island (Capo Verde) and M'Buor (Senegal)	9–29 September 2000	[68, 162]	*Ground-based:* - CIMEL Sun-photometers *Airborne:* - in situ sensors/radiometers /POLDER radiometer -backscatter lidar	Lidar/in situ measurements integration Dust in the PBL and up to 4.5 km Smaller radius in the PBL
ACE-Asia (Asian Pacific Regional Aerosol Characterization Experiment) http://saga.pmel.noaa.gov/aceasia	SE China, Korea, Japan (22–50°N, 100–150°E)	Spring 2001	[163, 164]	*Ground-based:* - Backscatter/Raman lidars - Sun photometer/Radiometers/Absorption Photometer *Airborne:* - AERONET Sun photometers/Radiometers/ PSAP/4 Nephelometer/In situ sensors *Shipborne:* Micro pulse lidar *Spaceborne:* - Aerosol and species retrievals	Depolarization measurements for discriminating spherical and no spherical particles Dust extinction coefficient at 532 nm up to 0.3 km^{-1}

Table 2: Continued.

Measurement campaign	Location	Period	Main references	Instruments	Lidar added value
MINATROC (Mineral dust and Tropospheric Chemistry)	Mount Cimone, Italy (44.2°N, 10.7°E, 1870 m a.s.l.) Izana, Tenerife, Spain (28.30°N, 16.48°W 2367 m asl)	June–July 2000 July –August 2002	[165]	- Differential mobility analyzer (DMA)/optical particle counter (OPC) - Single backscatter depolarization lidar	Dust layering 2–8 km a.s.l. Dust extinction coefficient $0.2\,km^{-1}$ (532 nm) Particle linear depolarization ratio ∼15% (532 nm)
CRYSTAL-FACE (Cirrus Regional Study of Tropical Anvils and Cirrus Layers-Florida Area Cirrus) http://cloud1.arc.nasa.gov/crystalface	SW and SE Florida, USA (24°–26°N 83°–80°W)	July 2002	[17, 166, 167]	*Ground-based*: - CIMEL Sun-photometers/Surface flux measurements/UV/IR/Broadband radiometers - Ceilometer - Backscatter lidars *Airborne:* - Sun-photometers/Radiometers/Nephelometer/In situ sensors *Spaceborne:* Aerosol and species retrievals	Dust particles are effective Ice Condensation Nuclei in mildly supercooled (−5.2/−8.8°C) altocumulus
UAE^2 (Unified Aerosol Experiment) http://uae2.gsfc.nasa.gov/	United Arab Emirates, Arabian Gulf and Gulf of Oman.	August–September 2004	[168, 169]	*Ground-based:* - 15 sun-photometers/AERI interferometer/particle sizer/NRL Mobile Atmospheric Aerosol And Radiation Characterization (MAARCO)/NASA's Surface-sensing Measurements for Atmospheric Radiative Transfer (SMART)/radiosonde - Micro pulse lidars *Airborne:* - Aerosol, clouds and water droplet probes/Cloud Absorption Radiometer/Polar Nephelometer - Lidar	Micro Pulse Lidar/Sun-photometer synergy: dust /clouds separation AOD at 550 nm AOD in IR in daytime Large AOD variability (range 0.4–0.53) Larger variability at coastal and island sites

Table 2: Continued.

Measurement campaign	Location	Period	Main references	Instruments	Lidar added value
AMMA (African Monsoon Multidisciplinary Analysis) http://www.amma-international.org/spip.php?rubrique1	Africa (Mali-Niger-Nigeria-Senegal-Benin-Algeria, Mauritania) (8°–19°N, 2°–8°E)	2002–2010	[71, 170–172]	*Ground-based:* - SW-LW broadband radiometers/AERONET/Microtops II Sun-photometers/TEOMs/Particle/CCN Counters/Aerosol filter sampling/Nephelometers/ Aethalometers/Pyranometers/Pyrgeometers/ Scatterometers/Pyrheliometers/Shadow band radiometers/Gas samplers (O_3, CO, SO_2, NO_x, COV) - Ceilometers/Elastic/Raman lidars/Depolarization/Raman lidars *Airborne:* - PSAP-PMS- FFSSP/Nephelometer/Q-AMS/ Shortwave Spectrometer (SWS)/Eppley radiometers/Solar Hemispheric Integrating Measurement System (SHIMS)/Gas samplers (O_3, CO, SO_2, NO_x)/Aerosol filter sampling	Mixing of dust with biomass burning particles (2–5 km) Dust extinction coefficient 0.2–0.4 km^{-1}, but also up to 1.5 km^{-1} (355 nm) Particle linear depolarization ratio 25% (355 nm) $S = 55 \pm 5\ sr^{-1}$ (355 nm)
SAMUM -1 (Saharan Mineral Dust Experiment) http://samum.tropos.de/	South Morocco Ouarzazate (30.9°N, 6.9°W, 1133 m a.s.l.) and Tinfou (30.2°N, 5.6°W, 680 m asl)	May–June 2006	([175] and references therein)	*Ground-based:* - in situ physical–chemical and optical sensors/AERONET Sun-photometers/ Radiometers/Radiosonde/Surface-sensing Measurements for Atmospheric Radiative Transfer (SMART)/Compact radiation measurement system (CORAS) - Raman lidars/Doppler lidar *Airborne:* - in situ sensors - HSRL	S (355 nm, 532 nm, 1064 nm) = 50–60 sr Particle linear depolarization ratio: ~30% (532 nm) Å(α) ~ 0 (355/532 nm) AOD < 0.8 (532 nm) Median effective diameter 2.5 μm CALIPSO underestimates the dust optical depth by about 25%. Lidar-AERONET comparison: - Good agreement for pure dust AOD and Å(α). -at near ultraviolet wavelengths differences in complex refractive index, lidar ratio and single scattering albedo

Table 2: Continued.

Measurement campaign	Location	Period	Main references	Instruments	Lidar added value
SAMUM 2 (Saharan Mineral Dust Experiment) http://samum.tropos.de/	Cape Verde, Africa ~15°N, 23.5°W	Winter 2008	[143, 155, 176]	*Ground-based* - in situ physical–chemical and optical sensors/ 3 AERONET Sun-photometers/radiometers/1 radiosonde - 3 Raman lidars/1 Doppler lidar *Airborne* - in situ sensors - HSRL	Dust layers depth (1.3 ± 0.4 km) Dust S (355 nm, 532 nm, 1064 nm): 50–60 sr Dust particles significantly aged

All of these properties were derived from multiwavelength lidar observations of pollution plumes mixed with dust particles advected from India and Southeast Asia out over the tropical Indian Ocean during the northeast monsoon.

The Puerto Rico Dust Experiment (PRIDE) took place in Puerto Rico between June 28 and July 24, 2000 and focused on improving the characterization of the optical, microphysical, composition, radiative, and transport properties of African dust (http://modis-atmos.gsfc.nasa.gov/PRIDE/). The main results of PRIDE [159, 160] showed that dust aerosols in the Puerto Rico region during the summer months result in a shortwave radiative cooling effect. In particular, diurnal means of $-12.34 \pm 9.62\,\mathrm{Wm}^{-2}$ at the top of the atmosphere and $-18.13 \pm 15.81\,\mathrm{Wm}^{-2}$ at the surface [161] were measured during PRIDE, showing that the Saharan dust aerosols have an important impact on large-scale shortwave radiation budget, and regional climate, also at thousands of kilometers from the source region. Moreover, the mid-visible AOD varied from clean marine conditions (0.07) to high dust loading periods (AOD > 0.5), while the average mid-visible AOD was 0.24. The NASA-GSFC micropulse lidar (MPL) available in Puerto Rico during PRIDE provided information about the vertical distribution of dust. Additional information was provided by airborne sunphotometers available during the campaign. The main output from the lidar measurements was that the dust vertical distribution in the Caribbean was found to be highly variable with both typical Saharan Air Layer (SAL) and lower level transport of dust being observed [67]. The SAL is a layer of warm, dry, dusty air, which normally overlays the cooler, more humid surface air of the Atlantic Ocean formed from late spring to early fall. According to the lidar measurements, dust frequently reached altitudes of 5 km. The presence of dust in the marine boundary layer was not correlated with any "typical" atmospheric sounding profile. In particular it did not correlate with the strength of the trade inversion in the Caribbean [67].

The Saharan Dust Experiment (SHADE) took place in the west coast of North Africa between 9 and 29 September 2000 and focused on improving the determination of the parameters that are relevant for computing the direct radiative effect due to dust particles. The airborne LEANDRE lidar [68] was used to derive the altitude of the aerosol layers. Vertical profiles derived from lidar measurements on September 25 highlighted the presence of the SAL located between 2.2 and 4.5 km with particle effective radii of $1.19 \pm 0.6\,\mu$m. Other dust layers within the sub-Saharan transition layer over the marine boundary layer were also observed, with particle radii significantly smaller than sizes within the SAL. The lidar technique provided local information about the geometrical height of the dust layers as well as about the size of the mineral dust particles. Observations collected during SHADE indicate a net cooling effect of dust particles in agreement with the model estimation of $-0.4\,\mathrm{Wm}^{-2}$ as global Saharan dust net direct radiative effect [162]. However, it has to be kept in mind that this estimation took into account only unpolluted dust, while dust particles are often mixed with biomass burning aerosols (the mixture is often referred to as polluted dust) occurring in Africa in the warm season.

Another very important international field campaign, involving multiple aircraft, ships, satellites, and surface sites, was the Asian Pacific Regional Aerosol Characterization Experiment (ACE-Asia), which generated the most comprehensive measurements ever collected of hemispheric aerosol emission and transport during springtime in 2001 [163]. The data acquired during ACE-Asia allowed a first-time assessment of the regional climatic and atmospheric chemical effects of a continental-scale mixture of dust and pollution in the whole region (http://saga.pmel.noaa.gov/Field/aceasia/). Lidar images of the normalized aerosol backscatter, extinction coefficient, and depolarization ratio at Beijing showed the advance of the dust storm over April 6–15, 2001, while automated Mie scattering lidar [164] was used to determine vertical profiles of backscattering intensities and depolarization ratios from near ground up to the two to six km height region. Lidar measurements of atmospheric depolarization were used to distinguish between spherical and nonspherical particles. Aerosol extinction at 532 nm reached values of up to $0.3\,\mathrm{km}^{-1}$.

Another important dust experiment, the Mineral dust and Tropospheric Chemistry (MINATROC) campaign, involving single wavelength polarization lidar observations took place at Mount Cimone in central Italy (44.2°N, 10.7°E, 1870 m above sea level (a.s.l.)) during June-July 2000 [165] and Izana, Tenerife (Spain) in 2002. In MINATROC lidar data were analyzed to derive tropospheric profiles of aerosol extinction, depolarization, surface area, and volume. Lidar retrievals for the 2170–2245 m level were compared to the same variables as computed from in situ measurements of particles size distributions, performed at the mountain top station (2165 m a.s.l.) by a differential mobility analyzer (DMA) and an optical particle counter (OPC). Lidar depolarization was observed to minimize mainly in air masses proceeding from Western Europe. Conversely, African, Mediterranean, and East Europe aerosol showed a larger depolarizing fraction, mainly due to coexisting refractory and soluble fractions. The data analysis showed average relative differences between lidar and in situ observations of 5% for backscatter, 36% for extinction, 41% for surface area, and 37% for volume, within the expected combined uncertainties of the lidar and in situ retrievals. Average differences further decreased during the Saharan dust transport event, when a lidar signal inversion model considering nonspherical scatterers was employed.

The Cirrus Regional Study of Tropical Anvils and Cirrus Layers-Florida Area Cirrus Experiment (CRYSTAL-FACE) campaign took place in July 2002 and was designed to investigate the physical properties and formation processes of tropical cirrus cloud (http://cloud1.arc.nasa.gov/crystalface/), including the potential of cloud-altering properties of transported Saharan dust. A new technique was developed within CRYSTAL-FACE to classify ice particles into different shape categories, based on lidar depolarization ratio. The data collected, using aircraft and ground-based polarization lidar [17, 166], showed that long-range-transported Saharan dust particles can act as ice condensation nuclei. In particular,

glaciation was observed in relatively warm altocumulus cloud (−5.2 to −8.8°C) close to the top of the desert dust layer [17]. The efficiency of dust particles as ice condensation nuclei was also observed for particles originated from Asian dust storm and transported towards western US [17, 166, 167], suggesting that major dust storms can affect the climate through indirect desert dust effect on cloud properties.

In the summer of 2004 (primarily August and September) the Unified Aerosol Experiment (UAE^2) field campaign was conducted in the United Arab Emirates and over the adjacent Arabian Gulf and Gulf of Oman. The focus areas of this field campaign included the characterization of fundamental physical and optical properties of atmospheric aerosol particles, the interaction of the regional/local meteorology with the aerosol radiative impacts, and the remote sensing of heterogeneous aerosol properties over the water and bright desert surfaces. During UAE^2 it was observed that the average diurnal variability of the AOD at 500 nm varied between sites (from 0.4 to 0.53), with the largest diurnal changes (from values lower than 0.2 to higher than 1) occurring at some coastal and island sites (probably associated with land breeze/sea breeze circulation). The 2-month average of the Ångström exponent ($a_{440–870}$) increased moving from the desert region: 0.50–0.57 at inland desert sites, 0.64 at coastal sites, and 0.77 over Arabian Gulf island sites [168]. This indicated that the observed dust particles are on larger average close to the source region. Correspondingly, the average fine mode fraction increased from ∼35% in the inland desert sites up to ∼48% in the Gulf island sites [168]. Lidars of the Micropulse Lidar Network (MPL-Net) provided the dust optical depths at 550 nm during this campaign, after calibration and using special software [169]. By comparing atmospheric emitted radiance interferometer (AERI) detection/retrieval results with collocated AERONET Sun photometer/MPLNET micropulse lidar measurements, it was thus shown that the synergy of AERI and lidar instruments could be used to separate dust from cloud and retrieve dust IR optical depths during daytime conditions.

The international multiyear African Monsoon Multidisciplinary Analysis (AMMA) program is an international research project involving field campaigns focused on improving the understanding of the West African Monsoon system [170]. Within this project, specific campaigns involving lidars were carried out: the Dust and Biomass-Burning Experiment (DABEX) [171] and the Dust Outflow and Deposition to the Ocean (DODO) one [172]. One of the results, related to lidar measurements [71], was that the vertical distribution of dust within the convective boundary layer was nonuniform and the occurrence of dust updrafts and cloud downdrafts intensified vertical recirculation within the Saharan atmospheric boundary layer (BL). Additionally, a strong dependence of the diurnal Saharan BL development on the season was observed ranging from 0.5 km in the wintertime up to 5-6 km height during the summer [71]. This was ascribed to the seasonality of several key features of the Saharan layer such as the amount of lofted dust, the humidity content, the large-scale subsidence, and the proximity of the Saharan Heat Low. Throughout 2006, the aerosol vertical distribution within the BL was nonuniform, with the majority of coarse particles being located near the surface. The aerosol content was influenced by dust transport from a variety of source regions after being lifted by different mechanisms (low-level jets; cold pools or topographic flows).

Combined ground-based and airborne lidars campaigns conducted during DABEX [70, 72] found thick layers of mineral dust aerosol in the local PBL (up to about 2 km). Elevated layers of biomass burning aerosol, mixed to a variable degree with dust, were found at altitudes of 2–5 km. Additional lidar experiments performed during AMMA [73] showed that the extinction coefficient within the dust layer ranged between 0.2 and 0.4 km^{-1} at 355 nm, and the linear particle depolarization ratio was around 25%. For some days when there was direct import of dust-loaded air masses from the Saharan desert, the extinction coefficient exceeded 1.5 km^{-1}. However, the vertical extent of such layers is only a few hundred meters. They also found layers of mixed dust and biomass burning aerosols with extinction coefficient within the same range of values. In their paper Heese and Wiegner [73] showed the importance of linear particle depolarization ratio measurements for discriminating between dust and biomass burning aerosols. This capability allowed them to characterize dust within biomass burning aerosol layers using the lidar ratio as an additional discriminator. In particular, a lidar ratio 55 ± 5 sr was typically observed in a Saharan pure dust layer during the dry season.

Yet, another dust campaign initiated in Asia as a joint Japan-China project, the Aeolian Dust Experiment on Climate impact (ADEC), took place from 2000 to 2006 in northwestern China [173]. However, the aerosol dust profiles obtained by lidars were limited to the derivation the aerosol backscatter coefficient and the structure of the lower troposphere during intensive observational campaigns.

Some recent data on Saharan dust observations over the Caribbean basin during the summer 2007 NASA Tropical Composition, Cloud, and Climate Coupling (TC4) field experiment are reported by Nowottnick et al. [174] involving the CALIOP lidar and the airborne Cloud Physics Lidar (CPL). In TC4 airborne the CPL and satellite observations from MODIS suggested a barrier to dust transport across Central America into the eastern Pacific. This barrier could be due to the dust transport dynamics, loss processes, or a combination of them. The NASA GEOS-5 aerosol transport model was used for investigating and defining the causes of the dust transport barrier. In these simulations, the best agreement with observations is obtained if it is assumed that dust particles are hydrophilic aerosols and act as cloud condensation nuclei. As a main result, it was found that loss processes by wet removal of dust are about twice as important as transport in producing the dust transport barrier [174].

Recently, the experimental campaigns of the Saharan Mineral Dust Experiment (SAMUM 1 and 2) [175] were conducted in summer 2006 and in winter 2008, respectively. The two campaigns were planned for investigating dust very close to the source region (SAMUM-1, southern Morocco) and in the outflow region (SAMUM-2, Cape Verde). These campaigns focused on the comprehensive characterization of pure mineral dust properties on the basis of a sophisticated

interplay between airborne and ground-based lidar/in situ instrumentation, augmented by ground-based sun photometers. For the first time, multiwavelength Raman/polarization lidars and an airborne high spectral resolution lidar were involved in major dust field campaigns and provided profiles of the volume extinction coefficient of the particles at ambient conditions (for the full dust size distribution), of particle-shape-sensitive optical properties at several wavelengths, and a clear separation of dust and smoke profiles.

Optical profiles of pure mineral dust were collected during a one-month measurement period in Morocco in 2006. Moderate optical depths of up to 0.8 at visible wavelengths characterized this period. Most interestingly, these cases describe pure mineral dust from ground level to heights of approximately 6 km. In situ ground and airborne observations show that the contribution of anthropogenic pollution, which mainly comes from traffic and agricultural activities in the field site area, is negligible. The profiles of Ångström exponents (355/532 nm) are around 0, which indicated the large fraction of coarse mode dust particles. Lidar ratios are mainly between 50 and 55 sr at 355 and 532 nm. Linear dust depolarization ratios are as large as 30% at visible wavelengths.

For the case of SAMUM-2, the aerosol layers were classified on the basis of HSRL and in situ measurements in 65 biomass burning and mineral dust layers [176]. Mineral dust layers typically were confined below 2 km of altitudes while biomass burning plumes were located at higher altitudes. Desert dust layers had a typical depth of 1.3 ± 0.4 km. In situ measurements showed a median effective diameter D_{eff} of 2.5 μm for the dust layers over Cape Verde. This value is significantly lower than the corresponding 5.9 μm obtained during SAMUM-1. The comparison between mineral dust size distributions as measured during SAMUM-1 and SAMUM-2 showed the aging of desert dust particles in SAMUM-2, with the removal of large particles and the increase of the center of the accumulation mode diameter as a result of coagulation.

During SAMUM-2, 31 tropical biomass layers were observed. These layers had a mean depth of 2.0 ± 1.1 km and were characterized by a median Å of 1.34. The related aerosol size distributions showed a significant amount of particles larger than 10 μm, that are mineral dust particles [176].

In terms of aerosol optical depth, the dust layers are responsible of a median AOD around 500 nm of 0.23 against the 0.09 AOD due to the biomass burning layers. Although the dust layers are thinner than biomass burning layers, their median contribution to the columnar AOD (below 10 km) is 75%, while 37% is the median contribution of biomass burning layers.

With regard to lidar measurement/techniques, observations performed during SAMUM showed that aerosol typing is possible based on depolarization and lidar ratios [155], and in situ measured absorption Ångström exponents [176]. The observations also showed that an improved characterization of nonspherical mineral dust particles is possible, if we use at least two measurement wavelengths [143].

4. Systematic Ground-Based Desert Dust Observations by Lidar

One of the main outputs of the last measurement campaigns related to dust is that lidar techniques are fundamental for aerosol typing, even if challenges still exist. This issue is even more complex away from the source region because mixing and modification processes affect aerosol optical and microphysical properties in a very complex way. Dust particles are typically transported thousands of kilometers from their source [10, 36, 38]. One of the more impressive and recent examples of long-range transport occurred in spring 2011, when an intense Saharan dust outbreak mobilized large amounts of dust from Northern Africa and was transported as far north as Norway over a weeklong period between April 3 and 10, 2011 [177].

As reported above, special measurement campaigns in the field are essential for characterizing the dust because of the large number of instruments and measurements which are deployed to support the field campaigns and are typically unavailable for routine measurements. Systematic observations performed far away from desert area are important for the assessment of the desert dust impact over large distances. In particular, systematic observations are important for quantifying the number of dust events, the typical altitudes, optical and microphysical properties, and finally the radiative impact.

According to the latest report of the Intergovernmental Panel on Climate Change (IPCC) [11], there is still a large uncertainty in the estimate of the effect on climate forcing of anthropogenic and natural aerosol. Previous studies demonstrated that a main cause of large uncertainties is the lack of an extensive climatology based on dust observations [18].

In the following sections, results based on long-term observations of dust are reviewed, distinguishing between two main regions of interest: Mediterranean-Europe and Asia. Lidar measurements of dust elsewhere are limited to few cases because of the low occurrence of dust intrusions (as in the case of continental US) and the paucity of lidar instruments (e.g., in Southern Hemisphere). Ferrare et al. [178] found that over 2 years of measurements by the operational Raman lidar in north central Oklahoma, only few cases may have been associated with the rapid transport of soil dust from the west and are characterized by low lidar ratio and high linear particle depolarization ratio. On the other hand, ceilometer measurements in east Australia, the largest dust source in the Southern Hemisphere, show that the large uncertainty of dust load in east Australian dust storms is mainly due to the absence of information about the vertical structure of dust plume [179].

4.1. Mediterranean-Europe. Many studies of Saharan dust intrusions over Mediterranean area are based on systematic measurements performed by passive satellite-borne sensors and ground-based sun photometers [37, 39–42, 180, 181], without information about the aerosol vertical distribution. Studies about the desert dust vertical distribution over the Mediterranean Basin are often based on episodic

measurements and case studies (e.g., [182–184]). Even if sporadic, these measurement studies showed the importance of lidar profiling capability for describing the complex dust vertical structure, with superposition of turbid layers from the surface to the free troposphere [183], significant changes in their vertical distribution within few hours [184], and an important horizontal variability [183]. The importance of low-level transport of dust was highlighted also for Middle East region where the availability of ground-based lidar measurements during two case studies combined with space-borne measurements and modelling tools, providing a new insight of the dust vertical distribution [185]. Tafuro et al. [184] also show that during strong events, the high values of the AODs dust particles are characterized by lidar ratios at 355 nm in the 50–70 sr range.

Measurements performed at individual lidar stations located in particularly interesting geographical site provide a better insight of the dust transport across the Mediterranean region (e.g., [86, 182, 186–188]). In some cases, systematic measurements are available allowing for long-term analysis (e.g., [86, 187]). For example, measurements performed from 1999 on the island of Lampedusa, in the central Mediterranean, at the Station for Climate Observations (SCO), showed the large presence of Saharan dust in the aerosol vertical distribution throughout the year, with a strong annual cycle both in aerosol vertical extension and optical depth [187]. Di Iorio et al. [187] find that over Lampedusa the desert dust generally reaches higher altitudes than other aerosol types, with a maximum monthly altitude of 8 km observed in spring.

Similarly to Lampedusa, the Azores are an optimal geographical location for dust observation during the transportation from Sahara toward American continent through the Atlantic Ocean, where airborne lidar measurements allowed the separation of the dust contribution from that of other aerosols [188]. Moreover, Chazette et al. [188] showed that a combined lidar and radiometry analysis is promising for retrieving the optical thickness of elevated dust layers as well as their spatial extent outside the source region even under cloudy conditions.

Finally, it was also found that in a big metropolitan area as Rome the dust particles advected in 30% of the days from Sahara over Rome strongly affect the typical aerosol load causing the exceedance of PM_{10} limits as established by the legislation for air quality [28].

Lidar measurements performed in the Mediterranean region show that the vertical structure of the aerosol in this region is typically very complex and stratified and that different aerosol types often coexist. If lidar measurements accurately retrieve the vertical structure of Saharan dust plumes, the combined use of lidar observations and satellite-borne sunphotometer measurements, regional dust models, and particle samplers is needed for investigating the dust complex behavior concerning its spatial and temporal evolution and mixing processes with other aerosol types along their transport routes [189].

Systematic observations of Saharan dust events over Europe are performed from May 2000 by EARLINET, the European Aerosol Research LIdar NETwork [61]. EARLINET is a coordinated network of stations that make use of advanced lidar methods for the vertical profiling of aerosols. At present (February 2012), the network includes 27 lidar stations distributed over Europe, as shown in Figure 3. EARLINET was established in 2000 with the main goal of providing a comprehensive, quantitative, and statistically significant database of the aerosol distribution on a continental scale. The backbone of EARLINET network is a common schedule for performing the measurements and the quality assurance of instruments/data [61]. EARLINET lidar observations are performed at each station on a regular schedule of one daytime measurement per week around noon (when there is a well-developed boundary layer) and two nighttime measurements per week (Raman extinction measurements), when the signal-to-noise Raman signal is higher [61, 190]. Further coordinated observations are addressed to monitor special events such as Saharan dust outbreaks, forest fires, photochemical smog, and volcanic eruptions.

Special care has been taken to assure data of highest quality possible. Therefore, all network stations participated in intercomparisons exercises both at instrument and algorithm levels with standardized procedures [191–193]. The data quality control establishes a common European standard for routine quality assurance of lidar instruments and algorithms and ensures that the data products provided by the individual stations are permanently of the highest quality possible.

Particular attention is paid to the monitoring of the Saharan dust intrusions over the European continent. The geographical distribution of the EARLINET stations is particularly appealing for the dust observation, with stations located all around the Mediterranean (from the Iberian Peninsula in the West to the Greece and Bulgaria and Romania in the East) and in the center of the Mediterranean (Italian stations) where dust intrusions are frequent, and with several stations in the central Europe where dust penetrates occasionally.

A suitable observing methodology has been established within the network, based on Saharan dust forecasts distributed to all EARLINET stations by the NTUA (National Technical University of Athens) group. The dust forecast is based on the operational outputs (aerosol dust load) of the DREAM (Dust REgional Atmospheric Model), and the Skiron models. The alerts are diffused 24 to 36 hours prior to the arrival of dust aerosols over the EARLINET sites. Typically runs of measurements longer than the typical 3-hour observations performed for the EARLINET systematic measurements are performed at the EARLINET stations in order to investigate the temporal evolution of the dust events. All aerosol backscatter and extinction profiles related to observations collected during these alerts are grouped in the devoted "Saharan dust" category of the EARLINET database. This category consists of about 4000 files (as of February 2012). This extended database permits the identification of suitable case studies involving several stations around Europe. Secondly, it is a unique tool for Saharan dust climatological studies on a continental scale.

Figure 3: Map of EARLINET (European Aerosol Research Lidar Network) stations. The number of the stations is continuously growing. The map reports the status at February 2012. Further stations in France, Germany, Israel, Georgia, and Turkey are going to join the network in the next future.

Case studies provide an opportunity to investigate dust modification processes during transport over the continent. For the first time, an optically dense desert dust plume over Europe was characterized coherently with high vertical resolution on a continental scale using observations performed at 10 EARLINET stations over southwestern, western, and central Europe during a strong Saharan dust outbreak in October 2001 [77]. Dust depolarization ratios at 532 nm, Ångström exponents at 355/532 nm, and lidar ratios at 355 nm within the dust layers mainly ranged from 15 to 25%, −0.5 to 0.5, and 40 to 80 sr, respectively. Lower depolarization ratio values indicate mixtures of anthropogenic and dust over some sites.

EARLINET measurements performed during the SAMUM-1 campaign permitted the investigation of the potential modification of dust optical properties from the source to continental Europe [194]. Different dust lidar ratios over Morocco and South Europe were found for the same dust case. Lidar ratios of 40–50 sr at 355 nm were measured over Italy and in Thessaloniki (GR), while values around 50–60 sr were measured at Morocco. Moreover, lidar ratios measured in Morocco are wavelength-independent values, whereas measurements at the lidar station at Potenza (IT) suggest slight wavelength dependence. Even if some variations of the dust lidar ratio are expected because potential modification processes occurred during the transport from Africa to Europe, mixing with anthropogenic pollution and maritime aerosol, are likely the main reason for that difference.

A first study on the impact of Saharan dust on European aerosol content was performed on the basis of all EARLINET data acquired during the first period of operation of the network (2000–2002) [79], documenting the horizontal and vertical extent of dust outbreaks over Europe.

A set of criteria was applied to identify the cases with Saharan dust intrusion [123]. The first criterion was that the aerosol profile should contain at least one distinct aerosol layer above the PBL [190] from all archived aerosol data. The second criterion was that the specific aerosol layer should originate from the Saharan region. The origin of this layer was identified using three-dimensional air mass back trajectory analysis. Finally, satellite data analysis, like TOMS

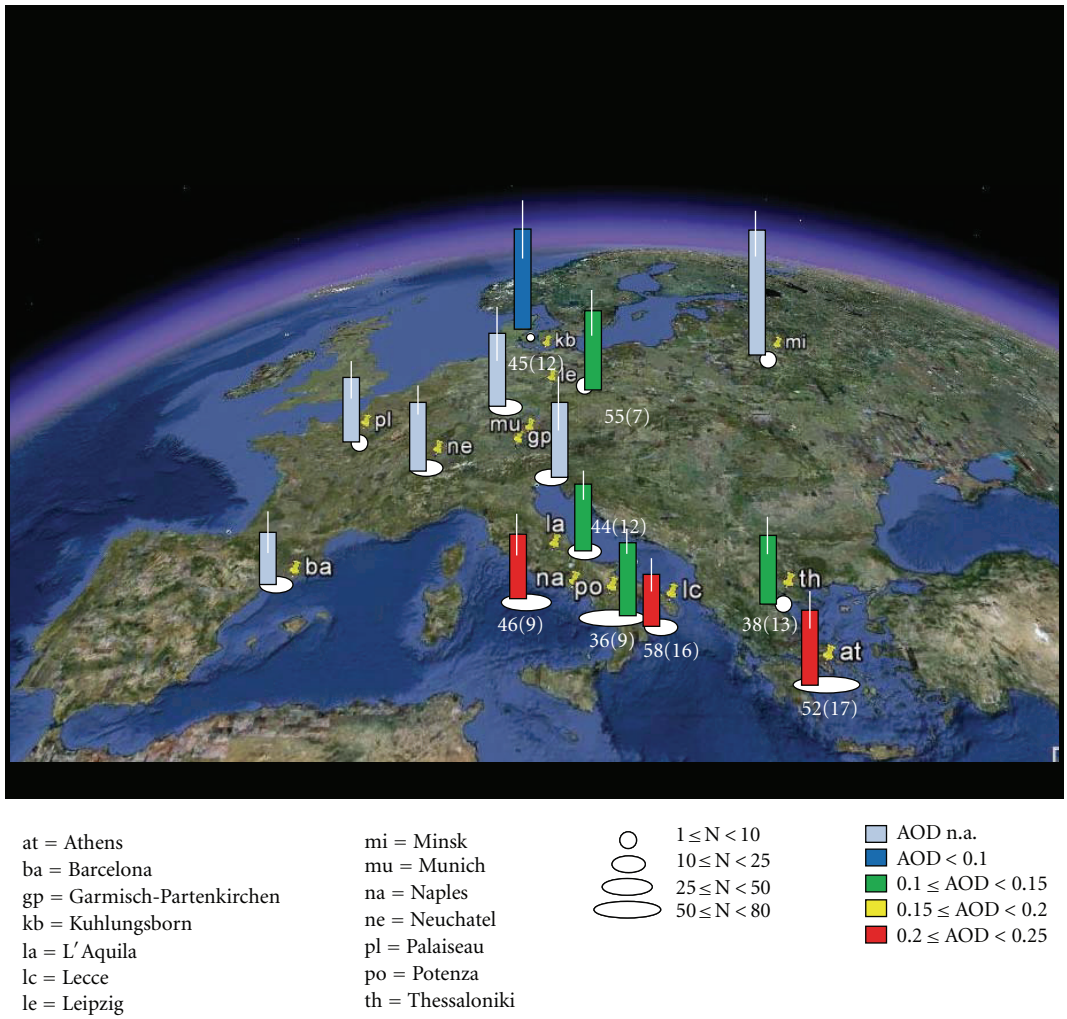

Figure 4: Main results of the 3-year climatological analysis performed within EARLINET [79]. For each station, the number of observed event (N) is reported following the code reported in the legend. The altitude of column bar represents the altitude of the dust layer center of mass and the white error bar its standard deviation. AOD at 355/351 nm is reported in different colors for different ranges of values. Finally, the mean S values at 355/351 nm calculated within the dust layer are reported in white followed by its standard deviation within brackets.

Aerosol Index and MODIS optical depth, has been utilized as ancillary information for identifying the cases in which air masses coming from the Sahara region carry lofted desert dust particles towards EARLINET sites.

In three years, about 150 days of Saharan dust outbreaks over Europe were monitored [79]. In most of the cases, episodes lasted from 1 to 5 days, while few of them lasted up to 7–10 days. Multiple aerosol layers of variable thickness, ranging typically from 1500 m to 3400 m, were observed at altitudes between 1100 and 9000 m a.s.l. Traces of dust particles have been observed in some cases up to 10000 m in Northern Europe [79].

The largest number of cases was recorded from late spring until early autumn months, while only few cases were observed during the winter period. However, the dust observations during autumn and winter cannot be negligible at least over Southern and Southeastern Europe. The number of dust episodes observed is much higher in the Southern and Southeastern regions as shown in Figure 4, mainly because of the proximity of these regions to the source region and to prevailing wind direction, while North and Western regions show low dust transport activity.

The mean altitude of the center of the mass of the dust layer identified above the PBL [123] is typically observed at about 3500 m a.s.l. (see Figure 4) [79]. Exceptions are found for the Barcelona (ES) and Lecce (IT) stations, where the dust layer is located around 2500 m, and for Minsk (BY) where it rises up to 6000 m. The mean AOD values at 351–355 nm inside the dust lofted layers (Figure 4) ranged over Europe from 0.1 to 0.25 with a standard deviation of the order of 20–100% that clearly indicates the high variability of the dust outbreaks over Europe. As reported in Figure 4, the mean S values ranged between 38 and 60 sr inside the dust layer, while their standard deviation is of the order of 20–30%. In northern Europe, linear particle depolarization ratio values range from 10 to 25% at 532 nm within the dust plume and

approximately constant Å($\beta_{355/532}$) values (−0.5 to 1) and high S values (30 to 80 sr) were found during the Saharan dust outbreaks. In southern and southeastern Europe a high S (20 to 100 sr) and Å($\beta_{355/532}$) (−0.5 to 3) variability was found, mostly related to the variability of aerosol microphysical properties (more cases are observed for Southern stations), and their probable mixing with maritime and anthropogenic aerosols along their trajectory from the source region to the observation site.

A first aerosol typing study [195] performed during the ESA-CALIPSO (EARLINET's Spaceborne-related Activity during the CALIPSO mission) study shows that among cases of Saharan dust intrusions observed over EARLINET in May 2008–October 2009 period, only 12% of cases can be considered pure Saharan dust cases, while in 88% of the cases, mixing of dust with different aerosol types cannot be excluded. The mixture of dust, pollution, and marine aerosol is the most frequently obtained. This can be explained by the large number of measurements for Mediterranean stations and by the presence in that region of marine aerosol, pollution, and dust due to the Mediterranean Sea itself, the European pollution, and the arrival of desert dust from Northern Africa, respectively.

Multiyear analysis performed at Mediterranean stations clearly showed the effects of this mixture of dust, pollution, and marine aerosol. A wide range of S at 355 nm values (20 to 100 sr) was observed over Thessaloniki (GR): S values as large as 80 sr correspond to the larger and more absorbing dust particles in agreement with nonspherical particles scattering calculations [110]. Values between 45 and 55 sr were found in most of the cases, in agreement with theoretical studies [111, 196], and finally values close to 20 sr are found in few cases where mixing with boundary layer urban and maritime aerosols makes the separation or even detection of dust in the lidar measurements difficult [197].

A trimodal Gaussian distribution was found for S at 355 nm measured within the desert dust layer (above the local PBL) over Potenza (IT) EARLINET station [123]. Each mode corresponds to different mixing: contamination between desert dust and maritime aerosols (mode centered around 22 sr), mixing between Saharan dust and aerosol typically present over Potenza (57 sr) and almost pure Saharan dust (37 sr).

A similar situation was found over Naples (IT), where the contribution of fine particles of local anthropogenic origin results in an S mode around 83 sr in the 0-1 km data besides another well distinct mode peaked around 34 sr, in agreement with Potenza (IT) typical value [198].

4.2. Asian Dust. As reported in the previous section, several field experiments (e.g., [161]) have been conducted over East Asia and the West Pacific to investigate the impacts of Asian dust. Combined in situ and lidar measurements indicate transport of aerosols in a shallow layer over the northern South China Sea that the Asian dust transported may have influence on air quality and marine ecosystems [199].

While in Europe dust intrusions occur mostly from early spring to late autumn [79], the period of highest occurrences

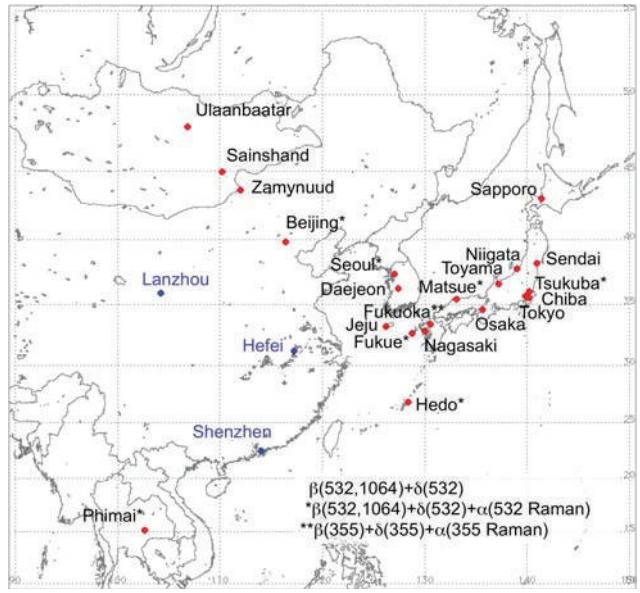

Figure 5: Lidar observation network in East Asia (AD-Net).

of dust storm over East Asia is the spring [163], with a secondary period of mineral dust outbreaks in East Asia in the fall [200]. Over the last few decades the number of dust days over East Asia showed an upward trend (Korea Meteorological Administration (KMA, http://www.kma.go.kr/), [201]). For example, the number of dust days in Seoul, South Korea, was 41 (period 1980–1989), 70 (period 1990–1999), and 106 (2000–2009) (KMA, http://www.kma.go.kr/).

Continuous observations of vertical distribution and optical properties of Asian dust in East Asia (China, Korea, Japan, and Mongolia) are made by depolarization and backscatter lidars with AD-Net. Figure 5 shows the current lidar locations in AD-Net.

Shimizu et al. [78] report on the occurrence frequency and the vertical distribution of dust particles on the basis of continuous operation of polarization lidars in Beijing (China), and Nagasaki and Tsukuba (Japan). Lidar observations are also carried out in South Korea [202] with the only multiwavelength Raman lidar in East Asia.

Regarding the Asian dust outbreak a common feature is the mixing of mineral dust with anthropogenic pollution [145]. Since much more coal and biomass are burned in Northeast Asia, Asian aerosol sources, unlike those in Europe and North America, add more absorbing soot and organic aerosol to atmosphere. The mixing occurs during the transport of the dust plumes from the Central Asian desert regions across the industrialized areas of China. The transport usually occurs in low heights and it is characterized by strong gradients of dust concentrations in the boundary layer. For example, PM10 measurements carried out by the KMA during record dust events of South Korea report particle concentrations of more than 1000 $\mu g/m^3$. Concentrations drop by a factor 4 within the first 250 m above ground [200]. As a result of the mixing processes it is difficult to measure important dust parameters of pure dust, that is, lidar ratios

and particle depolarization ratios. Kim et al. [203] report values of 0.84, 0.9, and 0.93 for single-scattering albedo for the wavelength range 530–550 nm during three Asian dust event periods over Gwangju, South Korea, in 2001. This SSA difference is explained by pollution coating. Eck et al. [204] report on cases where aerosol optical depth was predominately coarse mode dust aerosol in the spring of 2001. The authors find that absorption was greater in eastern Asia compared to the source regions, with ~0.93 of the average midvisible (around 550 nm) single-scattering albedo at Dunhuang, China (near the major Taklamakan dust source). This value was 0.04 higher than what was observed at Beijing.

Values of approximately 35% of the particle linear depolarization ratio are found as the current best estimate for the Asian dust [205]. Lidar ratios of dust particles are slightly higher at 355 nm (56 ± 10 sr) compared to 532 nm (51 ± 6 sr). The data are taken at Gwangju in South Korea. Measurements near Seoul (Anmyon Island) show values of 47 ± 7 and 45 ± 5 sr at 355 and 532 nm, respectively. The lower values may be caused by a stronger mixing of dust with marine aerosols over the marine lidar station or a stronger mixing of dust with urban pollution over Gwangju compared to what was found over Anmyeon Island. Additional observations of lidar ratios are given by [85, 206, 207].

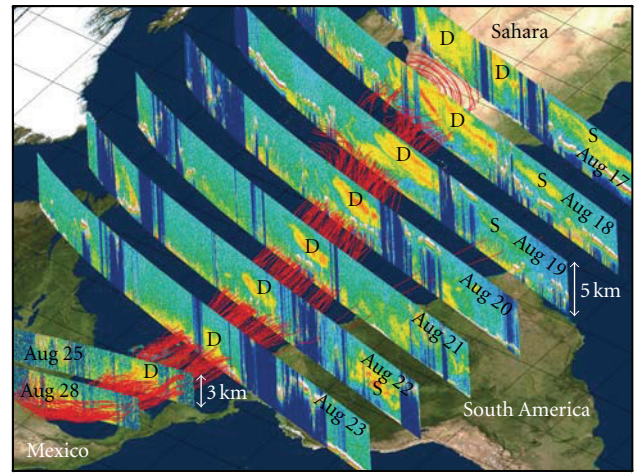

Figure 6: A figure reported in [80] shows an example demonstrating the capability of CALIOP to track dust long-range transport. A dust event that originated in the Sahara desert on 17 August 2007 and was transported to the Gulf of Mexico. Red lines represent back trajectories indicating the transport track of the dust event. Vertical images are 532 nm attenuated backscatter coefficients measured by CALIOP when passing over the dust transport track. The letter "D" designates the dust layer and "S" represents smoke layers from biomass burning in Africa (17–19 August) and South America (22 August).

5. Desert Dust Satellite-Based Lidar Observations

The launch of CALIPSO, the first satellite mission involving a lidar specifically designed to study aerosols and clouds, in 2006 ushered in a new era of space-based lidar measurements on a nearly global scale. The primary instrument aboard CALIPSO is the Cloud-Aerosol LIdar with Orthogonal Polarization (CALIOP) lidar, which is designed to acquire vertical profiles of elastic backscatter at two wavelengths (1064 nm and 532 nm) from a near nadir-viewing geometry during both day and night phases of the orbit [66]. In addition to the total backscatter at the two wavelengths, CALIOP also provides profiles of linear depolarization ratios at 532 nm, as defined in Section 2. Aerosol and cloud heights and retrievals of extinction coefficient profiles are derived from the total backscatter measurements [88, 208]. The depolarization measurements enable accurate discrimination between ice clouds and water clouds [209] and the identification of nonspherical aerosol particles such as dust [105]. These unique capabilities make CALIOP particularly suitable for measuring dust transport and vertical distribution, as demonstrated in Figure 6 [80].

CALIOP makes direct measurements of the attenuated backscatter defined as the product of the volume backscatter coefficient β and the square of the transmittance (T2) of the atmosphere between the lidar and the scattering volume (1).

In the current CALIPSO data release (Version 3), the cloud-aerosol discrimination (CAD) algorithm uses five-dimensional (5D) probability density functions based on these parameters: layer-mean attenuated backscatter at 532 nm, layer-integrated attenuated backscatter color ratio, altitude, feature latitude, and the layer-integrated volume depolarization ratio [210]. Adding the last two parameters to the CAD algorithm used in previous versions resulted in better separation between clouds and aerosols in the 5D space. In particular, the 5D algorithm has been designed in order to address, among other issues, the problem of misclassification of dense dust aerosol layers as cloud that sometimes occurred in previous releases [211]. Because CALIOP is a simple elastic backscatter lidar, the CALIPSO aerosol optical properties' retrieval currently most often relies on *a priori* assumptions to select an appropriate aerosol lidar ratio. The procedure for doing this is as follows. Once a layer is identified as an aerosol layer, its type is determined using the CALIPSO aerosol typing scheme [105]. This scheme operates in a three-dimensional space of lidar-derived information (feature height and feature-integrated values of depolarization and attenuated backscattering) taking also into account geographical location and surface type. Of the six aerosol types of the CALIPSO scheme, three (biomass burning, polluted continental, and polluted dust) use lidar ratios calculated from cluster analyses of multiyear (1993–2002) AERONET inversions [212]. Two models (marine and background/clean continental) were built either directly from measurements of size distributions and complex refractive indices or by adjusting model parameters to generate observed lidar ratio values.

Each of the CALIPSO aerosol types is characterized by lidar ratio distributions at both 532 nm and 1064 nm. Once the aerosol type of the layer is identified, extinction solutions are computed using the mean values of the lidar ratio distributions at 532 nm and 1064 nm. The variability of the lidar

ratio distribution (i.e., the standard deviation about the mean) is reflected in the extinction uncertainty profiles that are also reported in the CALIPSO data products.

In one important respect, lidar measurements from space-based platforms are quite different from ground-based or airborne measurements. For space-based systems, the very large distances between the lidar and its scattering targets (~700 km for CALIPSO aerosol measurements) result in a lidar footprint, that is, orders of magnitude larger than that of a ground-based or airborne system with the same receiver field of view [213]. The most immediate effect of this difference is that space-based lidar measurements are not accurately described by (1) and instead must explicitly account for multiple-scattering contributions to the backscatter signal [213, 214]. For CALIPSO, this is accomplished by introducing a multiple scattering factor, η, which modifies the particulate optical depth term in the single-scattering lidar equation [82, 208]. Among other things, the value of η used in any retrieval depends on the lidar sensing geometry and the scattering phase function of particles being measured. A reliable experimental determination of η has been established for CALIPSO measurements of cirrus clouds [89]. However, in the version 3 CALIPSO data products, aerosol multiple-scattering effects are considered to be negligible, and thus the aerosol extinction retrieval assumes single-scattering only from aerosol layers.

The CALIPSO classification scheme can identify two types of dust layers: pure dust and polluted dust. In this context, polluted dust is defined as a mixture of pure dust and biomass-burning smoke or anthropogenic pollution formed during dust transport [105]. Apart from polluted dust, no other mixtures are considered. Because the CALIPSO dust model is global in scope, regional differences with ground-based measurements can be expected. For example, comparisons with ground-based multiwavelength Raman lidar measurements of fresh Saharan dust over source region (Cape Verde) show that the aerosol extinction coefficients are underestimated in the CALIPSO products by about 30% [215]. Based on size distribution of dust particles from airborne in situ observations, it was shown that the discrepancies could be explained by the influence of multiple scattering, which is ignored in the CALIPSO retrievals. On the other hand, the CALIPSO backscatter retrieval works well and comparisons with ground-based observations show good agreement, because the lidar ratio value of 40 sr at 532 nm used for dust represents an effective value that accounts well for the reduced attenuation caused by multiple scattering in intense dust cases like that.

Despite the known limitations associated with the elastic backscatter measurement technique, since the inception of scientific measurements in June 2006, CALIPSO has acquired the largest amount of global dust data so far. The good quality of these data was proved through validation/comparison studies performed both at signal and optical properties levels using ground-based lidar stations as a reference (e.g., [211, 216, 217]). The CALIOP dataset provides an excellent opportunity for dust studies on a global scale. Based on the CALIOP measurements, comprehensive studies have been carried out on dust generation, transport (e.g., [80, 81, 218, 219]) and global or regional distributions (e.g., [80, 220]), and dust optical properties (e.g., [210, 221]).

Liu et al. [80] tracked an extensive dust storm from its origin in the Sahara dust to deposition in the Gulf of Mexico using CALIPSO data (Figure 6). Using CALIPSO backscatter measurements over the Sahara dust routes, Ben-Ami et al. [81] describe the differences in dust transport between the seasons and show a bimodal distribution of the average dust plumes height in both seasons. One of the most important contributions to global aerosol science of space-based lidars is the validation and enhancement of chemical transport models. Using vertically resolved attenuated backscatter from CALIPSO and AOD from MODIS, Generoso et al. [218] characterize Saharan dust outflow over the Atlantic and evaluate results from a global chemical and transport model (GEOS-Chem). All these pioneering studies were made possible after the launch and continuous operation of CALIPSO over the past nearly six years. In some cases (e.g., aerosol layers lofted over clear air or opaque aerosol layers), CALIPSO measurements have been used to estimate dust lidar ratios at both wavelengths as demonstrated in [221].

In the following, we briefly describe lidar ratio S measurements at 1064 nm derived from CALIPSO. In case of aerosol-free regions above and below a lofted cloud or aerosol layer, S can be calculated from the attenuated backscatter profile of an elastic lidar return [83]. As already reported, for layers that do not meet these qualifications an assumed value of the lidar ratio is needed for retrieving aerosol backscatter and extinction profiles from elastic backscatter lidar measurements, and the resulting uncertainties in the particulate extinction profiles and therefore the aerosol optical depth can be as high as of 30–40% [215]. It is therefore essential to have good estimate of lidar ratio. Because dust particles are nonspherical, theoretical estimates of lidar ratios obtained from scattering models have larger uncertainties for dust than for the nearly spherical urban pollution or marine aerosols. Additional uncertainties are introduced by the variability in the mineral compositions, particle size distributions, and shape parameters (e.g., aspect ratio and complexity factor), and all of which are highly variable and for the most part not well known. There are relatively few measurements or studies of dust S at 1064 nm [111, 153], therefore the S_{1064} are retrieved from CALIPSO data using optimization techniques discussed in [59]. The method requires a priori knowledge of S at 532 nm and a suitable profile of 532-nm attenuated backscatter amenable to the calculation of 532-nm aerosol backscatter coefficient profiles. A least-square method is applied to minimize the difference between the measured attenuated total backscatter at 1064 nm, and the same quantity as reconstructed from 532 nm profiles with specific S at 1064 nm and color ratio of 532/1064 nm. In this way, estimates of these last two quantities are obtained under the assumption that these characteristics do not vary substantially in the identified dust aerosol layer.

Figure 7 presents the occurrence frequency distributions of the effective lidar ratios S^* (i.e., the product of the naturally occurring lidar ratio and the instrument-specific multiple-scattering factor at 532 nm and 1064 nm) for opaque

Table 3: Dust optical properties from CALIOP and HSRL [80].

Date	CALIOP			
	18 August	19 August	20 August	HSRL: 28 August
Location	Northwest Coast of Africa	Atlantic Ocean ~1300 km from the coast	Atlantic Ocean ~2400 km from the coast	Gulf of Mexico ~7600 km away from the source
Vertical extent	1–6 km	1.5–5 km	2–5 km	1.5–3.3 km
$\tau_{532\,nm}$	0.6–1.2	0.3–0.45	0.29 ± 0.03	0.08–0.09
S_{532}	41 ± 3 sr	41 ± 4 sr	41 ± 6 sr	45.8 ± 0.8 sr
S_{1064}	52 ± 5 sr	55 ± 5 sr	54 ± 13 sr	44 ± 8 sr
β color ratio	0.74 ± 0.07	0.75 ± 0.08	0.72 ± 0.04	0.62 ± 0.01
$\tau_{1064/532\,nm}$	0.97 ± 0.02	1.01 ± 0.05	0.93 ± 0.17	0.62 ± 0.13
δ_p	0.31 ± 0.01	0.31 ± 0.01	0.32 ± 0.01	0.32 ± 0.01
Analysis method	Two wavelengths for 1064 nm	Two wavelengths for 1064 nm	Opaque water cloud For 1064 nm	Two wavelengths for 1064 nm

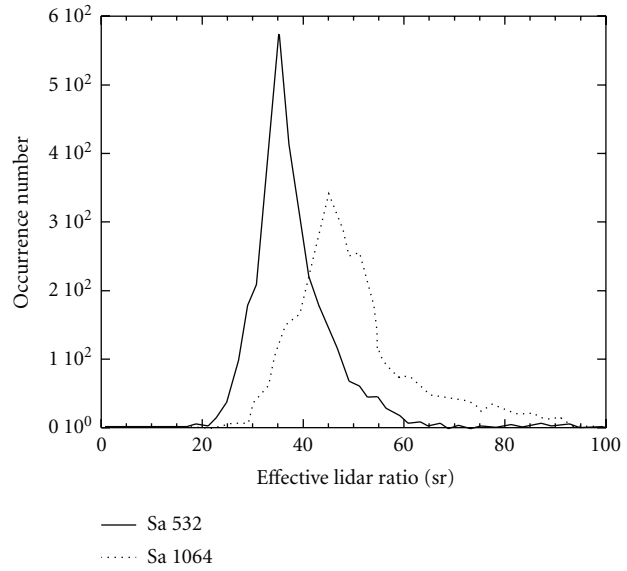

Figure 7: Occurrence number of effective lidar ratios (the product of the naturally occurring lidar ratio and the instrument-specific multiple scattering factor at each wavelength) at 532 nm and 1064 nm for African dust derived from the first two and a half years of the nighttime CALIOP data acquired over land within a geographical region of (12°N–30°N, 30°W–35°E) in the North Africa. The median/mean is 36.4/38.5 ± 9.2 sr at 532 nm and 47.7/50.3 ± 12.3 sr at 1064 nm. Figure from [210].

aerosol layers for a region between 12°N to 30°N and 30°W to 35°E in the North Africa where pure dust is the dominant aerosol. The retrieval is based on the fact that when a layer is opaque, the effective lidar ratio can be approximated as $S^* \approx (2\gamma')^{-1}$, where γ' is the layer integrated attenuated backscatter from the layer top to the apparent base. Thus, this parameter can be calculated directly from the measured attenuated backscatter. The median/mean value of S^* is 36.4/38.5 ± 9.2 (sr) at 532 nm and 47.7/50.3 ± 12.3 (sr) at 1064 nm. The 25th and 75th percentiles are 32.3 and 40.7 at 532 nm, 41.4 and 53.5 at 1064 nm, respectively. The depolarization ratio (δ_p) is 0.3 ± 0.07. These median/mean values are little bit smaller (<10%) than those derived in the previous case studies for moderately dense dust layers [80, 221]. Multiple scattering may have contributed to the observed smaller values, because the dust layers considered in this study are opaque and optically dense [210]. Table 3 adopted from [80] shows typical Saharan dust properties as measured by CALIOP over the Atlantic Ocean and concurrently with HSRL in the Gulf of Mexico.

6. Models/Observations Cooperation

SDS-WAS promotes a closer cooperation between modelers and observation communities [20]. The main reason for this is that an intercomparison between the leading aerosol models [222] found high diversities in the models for the removal rate coefficients and deposition pathways of dust. The assimilation of observations in model modules will probably improve their performances. Therefore, both comparison and assimilation of observations with models are fundamental for improving dust forecasts. In this context, lidar observations would play a leading role because of their vertical profiling capability. Some comparisons between lidar profiles and forecast models were performed for special cases like volcanic eruptions (e.g., [134, 223, 224]) and selected Saharan dust events (e.g., [197, 225, 226]). First efforts in this sense are really promising, even if they also show some weaknesses of these integrated approaches.

In the following, we report some significant examples of systematic dust model evaluation and assimilation efforts. They are mainly related to the 2 nodes of the SDS-WAS, the Northern Africa-Middle East-Europe Node and the Asian Node, respectively.

The large database of high quality Saharan dust observations provided by EARLINET [79] is the best candidate for a systematic comparison with dust model outputs aimed at the evaluation of dust models performances over the European continent, that is, over a large area characterized by different aerosol content regions (Mediterranean, continental Europe, Northern Europe, and Eastern-polluted countries). The outputs of the DREAM model were used in a first comparison [227] because they are provided for each EARLINET site

every 6 hours in terms of maps of the dust loading over the Mediterranean Sea and dust concentration profiles. A method for a quantitative evaluation of the dust-modeled profiles was explored starting from the Potenza (IT) station (see Figures 3 and 4) selected as the site with the largest database of dust profiles (on average once every ten days there is a Saharan dust intrusion in the vertical column over the site) [79, 123]. The evaluation method was specifically designed and optimized for providing a comparison in terms of dust layer geometrical properties (base, top, extension, and center of mass) and of dust concentration/optical properties. The realized software accepts as input every backscatter or extinction file in the EARLINET netcdf standardized format. In principle, the forecast profile provided by any model can be ingested with minor modifications to the code in some cases. The evaluation of models through lidar observations poses three main questions: how can quantities with different temporal resolution (30 minutes and 3 hours, for lidar and DREAM respectively) be compared? How can the high vertical resolution of lidar data (order of 100 m) be used in the model low-resolution (up to 1 km) profile evaluation? How is the PBL treated when there are other kinds of aerosols present?

The evaluation method developed for this first study specifically addressed each one of these critical issues as follows: (i) performing comparison both with the closest in time model profile to the median time of observations and the average over 9-hour time slot of model output, (ii) adapting the observation profile to the model profile, and (iii) including a specific system in the routine for excluding the PBL region by the comparison starting from the PBL estimation provided by the observations.

This methodology was applied to more than 150 dust profiles collected at the Potenza-EARLINET station over 5 years of measurements. Comparison shows good performance of the DREAM model in describing the vertical structure of dust layers. Differences between the center of mass of the layer as forecasted and observed are on average 0.1 ± 1.6 km. Figure 8(a) reports the count distributions of the center of mass as truly observed and forecast for Potenza site. Similarities between the two distributions plus the case by case agreement demonstrate that the forecast center of mass adequately reflects the observed one in terms of mean value, variability, and distribution. Larger differences were instead found for the base and top of the layers, which are due to the local aerosol affecting low altitudes and sensitivity-related aspects, respectively. More about these first results can be found in Mona et al. [227]. A further output of this first model evaluation attempt is related to the extinction-to-mass conversion factor. As reported above, this factor is not well known and is critical for aviation and air quality when there is a need to convert lidar extinctions to mass concentrations. The DREAM model actually assumes that for dust cases a simple, unique number could be used for translating concentration profiles (as those provided by DREAM) into extinction profiles (as EARLINET ones). The simple comparison between these 2 quantities (see Figure 8(b)) clearly demonstrated the limit of this kind of assumption: a mean value could be used for the whole dataset but this would lead to large uncertainties (widely spread values) when used for specific cases, as would be the case for specific aviation or air quality purposes.

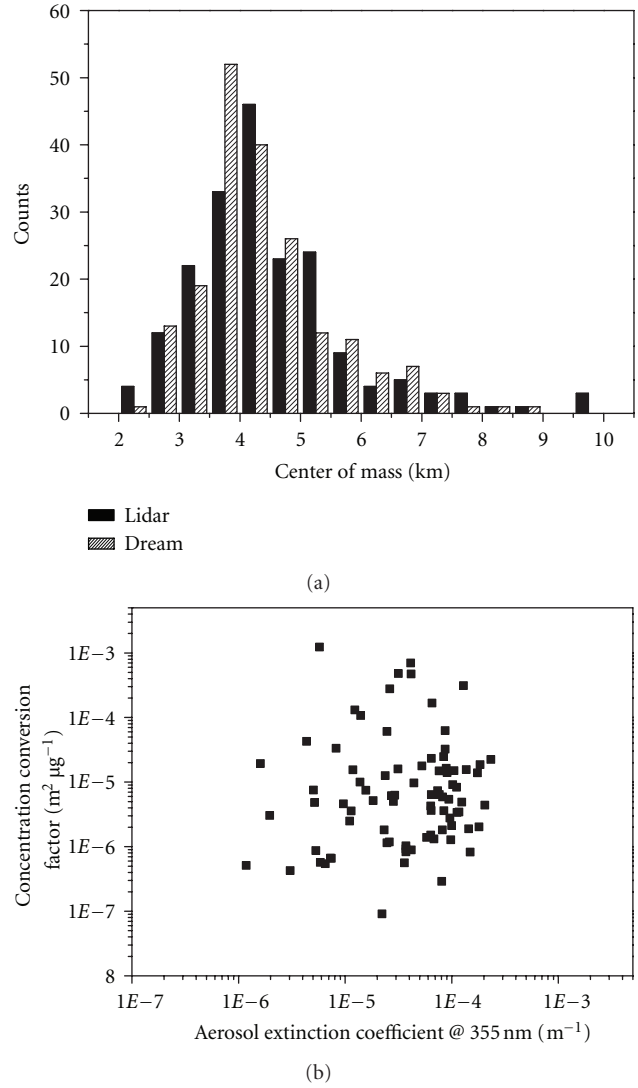

Figure 8: Results of DREAM evaluation through EARLINET measurements performed over Potenza [227]: counts distribution of center of mass of the identified Saharan dust layers (a) and evaluated concentration conversion factor as a function of the extinction coefficient as measured by lidar (b).

Data assimilation is commonly used in meteorological modeling for weather forecasting and reanalysis. However, application of data assimilation methods to chemical transport model is relatively new. The first data assimilation of mineral dust with ground-based lidars was reported by Yumimoto et al. [228]. They developed a four-dimensional variation (4DVAR) data assimilation system for the ground-based network (AD-Net) and performed assimilation experiments for several Asian dust cases [74, 219, 228, 229]. It was demonstrated that the data assimilation was useful not only for better reproduction dust distribution but also for better estimates of dust emission in the dust source regions.

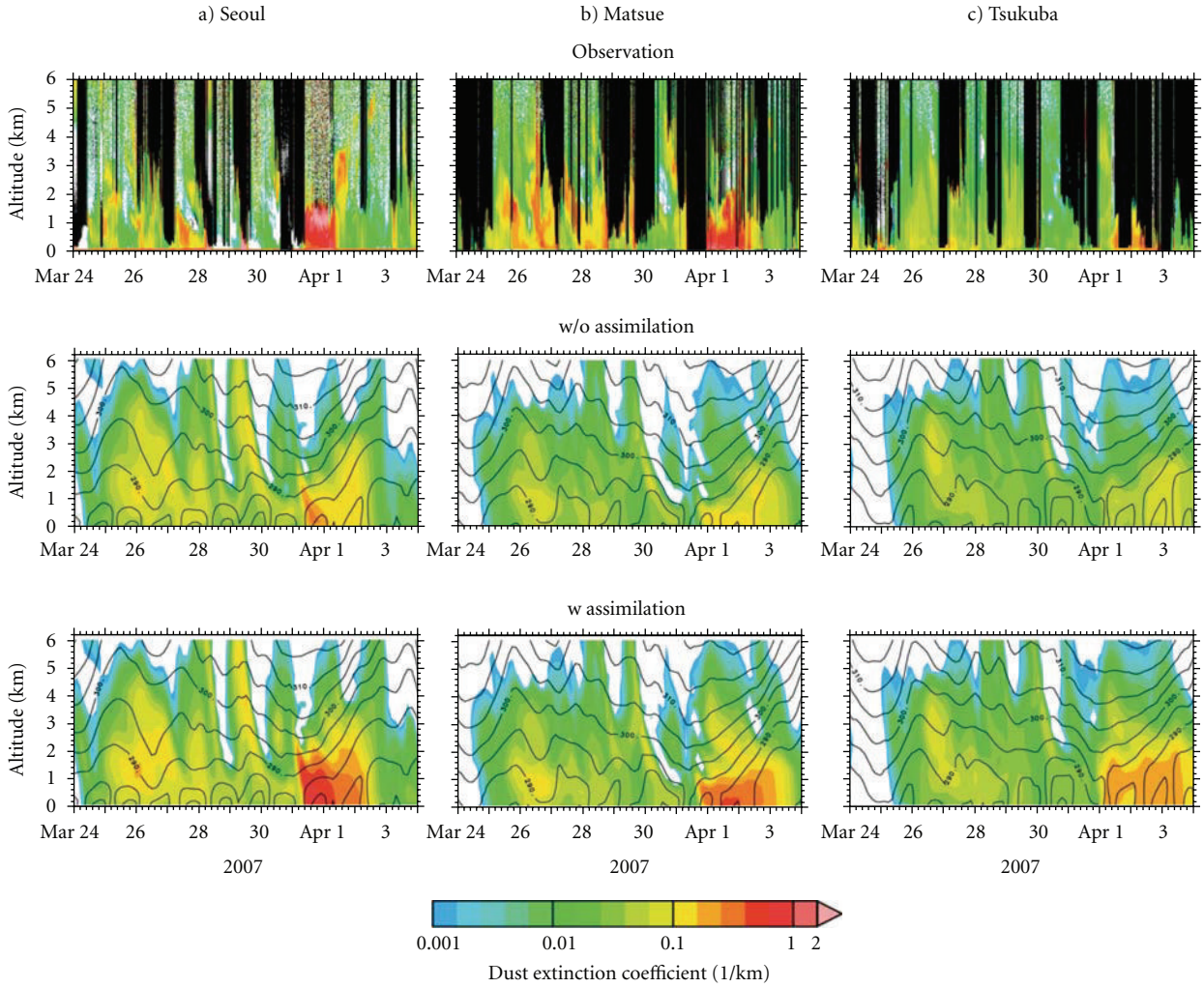

FIGURE 9: Time-height indications of dust extinction coefficient at Seoul (KR), Matsue (JP), and Tsukuba (JP). The first row shows observation. Second and third rows show modeled dust extinction coefficient without and with data assimilation. Figure from [229].

The data assimilation system developed by Yumimoto et al. [229] is based on the 3D real-time regional scale chemical transport model coupled with the Regional Atmospheric Modeling System (RAMS) [230]. In the dust data assimilation, a scaling factor was introduced in the dust emission function as the control parameter to optimize daily dust emission at each grid. The scaling factor can represent changes in surface conditions such as vegetation growth that are not considered in the original model. The size distribution of dust emission was not changed in the data assimilation.

The dust extinction coefficient profiles at 532 nm derived from the two-wavelength (1064 nm, 532 nm) polarization sensitive (532 nm) backscattering lidars in AD-Net were used for the data assimilation. The dust extinction coefficient was derived with the following procedure. First, dust layers were detected, and the extinction coefficient was derived using a constant lidar ratio ($S = 50$ sr). Then the contribution of mineral dust in the extinction coefficient was estimated on the assumption of simple external mixing of nonspherical dust and spherical aerosols using the depolarization ratio [78, 164]. An error analysis showed that both the error caused by uncertainty in S and the error in estimating dust mixing ratio converge in dense dust condition [231]. One-hour-averaged dust extinction coefficient profiles up to 6 km height were used with a 3-hour interval in the data assimilation.

Figure 9 shows time-height indications of dust extinction coefficient at three locations derived from the lidars, calculated with the model without assimilation and with assimilation. As can be seen in Figure 9, the dust event is better reproduced with the data assimilation. The improvement is natural because the data at these locations were used in the data assimilation. However, the two-dimensional distribution of dust optical depth was also much improved, and it agreed better with satellite data (OMI AI and MODIS AOD). The comparison with surface concentration data also showed the improvement with the data assimilation [232].

The assimilated dust extinction coefficient also agreed well with the CALIPSO dust extinction coefficient derived with the same data analysis method.

Sekiyama et al. [233] reported data assimilation of CALIPSO data using ensemble Kalman filter method. They used the attenuated backscattering coefficient and the volume depolarization ratio successfully for the data assimilation. However, it is difficult to use the attenuated backscattering coefficient in data assimilation of ground-based lidars, because the model must reproduce aerosol concentration (not only dust) accurately in the lower atmosphere. The use of the dust extinction coefficient is therefore reasonable for dust data assimilation with ground-based lidars. In the studies introduced above, the simple one-wavelength method for estimating the dust extinction coefficient was used.

For the AD-Net lidars, a method based on a spheroidal dust model using the signal intensities at 1064 nm and 532 nm and the volume depolarization ratio at 532 nm can be applied [234]. Data analysis methods including independent extinction coefficients measurements with high-spectral-resolution lidars (or Raman lidars) are also developed to derive the extinction coefficients of various aerosol components. The use of such methods will improve the estimation of the dust extinction coefficient, though the problem with detailed characteristics of dust that may depend on source regions and the problem with internal mixing during transport will still remain. If aerosol models in chemical transport models improve to handle these problems, it will be reasonable to use the extinction coefficients, the backscattering coefficients, and the particle depolarization ratios measured, for example, with HSRLs (such as the EarthCARE-borne lidar) for data assimilation.

7. Lidar Observations and Results about Dust-Related Risks

SDS-WAS recognizes the important role played by both observations and models in providing services that can be used to substantially reduce risk of various dust impacts [20]. Among the others, air quality deterioration due to dust and its effects on health and dust impacts on transportation could be effectively addressed by lidar techniques.

7.1. Air Quality Management. Because of the potential impact of aerosol, in particular submicron ones, on health, many countries have adopted air quality standards for airborne particulate matter (PM). An important application of dust forecasting to air quality management is found in southern Europe. Elevated Saharan dust PM in air masses transported from North Africa to countries of Southern Europe often exceeds the PM_{10} limits established for air pollution by the European Directive. The European Directive 2008/50/CE allows subtraction of PM exceedances caused by natural events from statistics used to determine air quality of EU sites. At the present time, there are only few studies addressing the issue of the effective determination of desert dust contribution to PM measurements on systematic basis [28–30, 235, 236]. In particular, the origin of the daily PM_{10} exceedances in regional background stations of the Iberian Peninsula was investigated in [235, 236] focusing on Saharan dust intrusions, using back-trajectory analysis and available PM model outputs in conjunction with satellite data and meteorological maps. As one of the first systematic studies on PM natural contribution, these papers are the main scientific basis for the guidelines provided by the European Commission for demonstration and subtraction of exceedances attributable to natural source [237]. After the identification of the natural source (in this case Sahara region) through models (trajectories and chemical transport models) and satellite images (no quantitative data), the contribution of Saharan dust to PM_{10} levels is quantified from the running average levels of PM_{10} measured in rural background stations in the days not affected by Saharan intrusions. Furthermore, recent studies show an impact of Saharan dust also on smaller particles even on the PM_1 fraction, which could have stronger impact on human health than larger size particles (e.g., [238]).

Many aspects are not yet addressed and considered at all by the methodologies provided in the guidelines. Among the others, (1) European countries characterized by high population density are often not equipped with suitable rural background stations, necessary for the subtraction proposed methodology, (2) spatial representativeness of background sampling point is not investigated, (3) long-range transported aerosols that affect free troposphere altitude range and then intrude in the PBL are often not considered in the evaluation of the impact on local air quality, and (4) that the interregional and international transport of pollution PM is not taken into account.

An integrated study of air quality based on long-term ground-based and satellite measurements of aerosols could address all these points. Particularly innovative in this context is the combined use of advanced lidar techniques with other PM measurements [21, 28, 33]. The long-range transported aerosols can be deposited into the PBL of the region and influence the surface PM. Forecasts by models and back-trajectories show these effects though these are highly uncertain in the PBL region. High vertical and temporal resolution lidar measurements of profiles of aerosol optical properties provide detailed information about the aerosol layering and in principle can provide the exact timing of the intrusion of upper level aerosol layers within the PBL. This could permit taking into account that long-range transported aerosol is present at different altitude levels.

Satellite quantitative data and a mathematical approach could be used for addressing in a quantitative way the horizontal representativeness of the data provided by the PM monitoring network. Particularly important for the operational application of such methodology is the assessment of ceilometer use for the layering identification through the comparison with advanced lidar measurements. This could also provide the basis for the improvement of monitoring networks through the addition of automatic low-cost instruments (such as sunphotometers and ceilometers) besides the PM samplers. To achieve these objectives, many efforts are currently in progress at infrastructural level, for example, within ACTRIS (Aerosols, Clouds and Trace gases Research

InfraStructure Network), EU FP7 project, and by means of European Commission financial instruments. An example of the latter is the EC LIFE+ project "DIAPASON" (Desert-dust Impact on Air quality through model-Predictions and Advanced Sensors ObservatioNs). DIAPASON, started on September 2011, applied an integrated approach between research-type polarization lidar, suitable ceilometers developed within the project, PM observations, and open-access model forecasts for attesting and assessing the effects of Saharan dust advections on European PM levels [239].

7.2. Transportation. Visibility-reducing dust storms are common in desert regions and a hazard to highway safety. Desert dust or volcanic ash can cause significant problems in aviation by reducing visibility and causing engine mechanical problems such as erosion and corrosion.

Desert dust and volcanic ash particles impact and bounce on cold areas of the engine, causing surface damages and deterioration and gradual loss of performance of the engine [35]. The problem is more severe in the case of volcanic ash due to their irregular shape and sharp edges. However, desert dust particles as well as volcanic ash can lead to false flight speed reading. This may be extremely hazardous especially in low-level flight such as during takeoff or landing procedures. The ingestion of these particles has impacts on the aircraft performance that are not fully explored yet for the aerospace industry. Sand and dust storms occur much more often than volcanic eruptions and affect aviation operations in many places on the Earth with significant safety and financial implications. For this reason, flight paths and flight management in dusty environments must be reassessed using more information and observations of the concentration and composition of the suspended aerosol. A critical issue in this assessment is deriving the mass-to-extinction conversion factor for the different tropospheric aerosol types. During the volcanic eruption in Iceland on April-May 2010, there was a strong request for knowing the mass concentration of volcanic particles. Answering to this request, mass-to-extinction conversion factor for fresh ash was derived by different authors [240, 241]. Regarding dust, a first attempt was reported in Barnaba and Gobbi [42] where an estimation of this conversion factor is provided for three aerosol mass types: marine, dust, and continental aerosols on the basis of size distributions and refractive index typical for each aerosol type and some aerosol extinction lidar measurements. After that, other papers addressed the issue of mass-to-extinction conversion factor (e.g., [231, 242]). However, there are still large uncertainties in estimates of conversion factors. These uncertainties are not well quantified. Even if the conversion factors work well for a specific case whether they can be applied to other situations still needs to be investigated in detail.

8. Concluding Remarks and Future Perspectives

In the last 30 years, lidar observations of atmospheric desert dust particles have given a better insight into the 4D distribution dust and its optical properties, investigating on a global scale previously hidden features: the vertical layers and associated properties. Lidar dust observations revealed a complex vertical distribution of mineral particles, with dust particles reaching altitudes up to 10 km in multilayer structures, and with dust particles often mixed with aerosol of different types and modified during transport from the source region. In addition, lidar measurements collected worldwide highlight the high variability of dust optical and microphysical properties. Intensive properties, those that depend only on the type of dust, are highly variable even for each site and for each event, in particular in the vertical profile.

Means and modes of dust investigation by lidar evolved over the years as instrumental technologies developed and observational capabilities improved. In this paper, this progress is described in a sort of historical *excursus*, describing aerosol lidar techniques from the simplest to the state-of-the-art. The paper summarizes results obtained from lidars employed in measurements campaigns from 1990s and presents climatological records from the Mediterranean and Asian regions since the beginning of the 21st century. A novel aspect of lidar investigation of desert dust is its application for societal benefits and risk management. This moves the lidar community from science research towards the potential applications communities. Although there has been significant progress achieved in such relatively short period from both technological and observational points of view, there are still specific weaknesses and gaps to address and overcome. Among these, three major points can be identified.

First of all, there are some gaps in the observational capability in horizontal and temporal dimension. Lidars provide high resolution measurements in the temporal and vertical dimensions but their geographical distribution is limited by a very narrow footprint and is not sufficient for global coverage. The CALIPSO satellite-borne lidar is limited in temporal coverage because of its repetition cycle. The more widely distributed ceilometers could be used to improve the lidar horizontal coverage. To achieve this, however, it is essential to assess ceilometer performances in comparison to lidars. Currently, this point is under investigation worldwide: first comparison studies were carried out with lidar and ceilometer collocated observations [125–127], while the use of ceilometer as tool for air quality monitoring is investigating within DIAPASON [239] through the ceilometer/lidar comparison.

Secondly, weaknesses related to aerosol lidar techniques, like the absence of complete overlap in the lowest atmosphere, the low SNR for Raman signal, and the required assumptions for elastic backscatter lidar retrievals, result in nonnegligible errors in lidar-retrieved dust properties. On the basis of the first promising results, it is expected that the systematic comparison and integration with different instruments such as sunphotometers and radars could reduce these uncertainties and furthermore could give a better insight of dust particle microphysical properties and interaction with clouds.

Finally, lidar measurements are typically not exploited by nonpractitioners of lidar though both the fundamental

measurements (e.g., aerosol layering) and secondary products (e.g., aerosol type, AOD, mass) are of importance to some of these communities (e.g., air quality scientists, aviation advisory personnel, and weather forecasters). A critical hurdle to achieve wider use is that often lidar data are not available in short time, while near real-time would be essential for model assimilation and air quality monitoring and forecasts.

The SDS-WAS plans for the next 5 years specifically address these points. In particular, with respect to lidar activities the following actions are foreseen for the next 5 years [20]: coordination of the observational networks, integration between other instruments, near real-time data delivery, and evaluation/assimilation of models.

SDS-WAS stimulates and promotes all these activities and supports and participates in dust-related projects. Observations of sand and dust are made by many agencies and are being coordinated globally through the GAW programme as part of a WMO Integrated Global Observing System. In particular, GALION aims to coordinate worldwide lidar observations in order to provide the vertical component of aerosol distribution [64]. The coordination of European ground-based network of stations equipped with advanced atmospheric probing instrumentation for aerosols, clouds, and short-lived trace gases is the main objective of ACTRIS (Aerosols, Clouds, and Trace gases Research InfraStructure Network), an infrastructural project of EU FP7 (2011–2015). Within ACTRIS, integration with sunphotometers will be investigated for improving daytime lidar observational capability and aerosol microphysical properties retrieval, and lidar/radar combined approaches will be exploited for aerosol and clouds interaction studies (http://www.actris.org/). Evaluation/assimilation of dust models through lidar data is envisaged in the next 5 years under the umbrella of SDS-WAS. In this context, it is particularly interesting the Monitoring Atmospheric Composition and Climate (MACC) EU project. MACC is an initiative of Global Monitoring for Environment and Security (GMES). GMES-MACC (http://www.gmes-atmosphere.eu/) extracts information from as wide a range of observing systems as possible and combines the information in a set of data and graphical products that have more complete spatial and temporal coverage and are more readily applicable than the data provided directly by the observing systems. At European level, the optimisation of EARLINET data processing [243] will provide an important step for near real-time data delivery and for models' evaluation/assimilation.

Acknowledgments

The authors would like to acknowledge Google map and Google Earth for the images used for realizing Figures 2, 3, and 4 reported in the paper. The financial support for EARLINET by the European Commission under Grant RICA-025991 and by the European Community through the ACTRIS Research Infrastructure Action (7th Framework Programme—ACTRIS Grant Agreement no. 262254) is gratefully acknowledged. The authors also acknowledge the ESA financial support under the ESTEC contract 21487/08/NL/HE. Work at GIST was funded by the Korean Meteorological Administration Research and Development Program under Grant CATER 2012-7080.

References

[1] S. Kinne, M. Schulz, C. Textor et al., "An AeroCom initial assessment—optical properties in aerosol component modules of global models," *Atmospheric Chemistry and Physics*, vol. 6, no. 7, pp. 1815–1834, 2006.

[2] C. S. Zender, R. L. Miller, and I. Tegen, "Quantifying mineral dust mass budgets : terminology, constraints, and current estimates," *Eos, Transactions, American Geophysical Union*, vol. 85, no. 48, pp. 509–512, 2004.

[3] U. Dayan, J. Heffter, J. Miller, and G. Gutman, "Dust intrusion events into the Mediterranean basin," *Journal of Applied Meteorology*, vol. 30, no. 8, pp. 1185–1199, 1991.

[4] R. A. Duce, "Sources, distribution and fluxes of mineral aerosols and their relationship to climate," in *Aerosol Forcing on Climate*, R. J. Carlson and J. Heintzenberg, Eds., pp. 43–72, John Wiley & Sons, New York, NY, USA, 1995.

[5] I. Chiapello, G. Bergametti, B. Chatenet, P. Bousquet, F. Dulac, and E. Santos Soares, "Origins of African dust transported over the Northeastern tropical Atlantic," *Journal of Geophysical Research*, vol. 102, no. 12, pp. 13,701–13,709, 1997.

[6] B. Marticorena, G. Bergametti, B. Aumont, Y. Callot, C. N'Doumé, and M. Legrand, "Modeling the atmospheric dust cycle 2. Simulation of Saharan dust sources," *Journal of Geophysical Research*, vol. 102, no. 4, pp. 4387–4404, 1997.

[7] J. M. Prospero, P. Ginoux, O. Torres, S. E. Nicholson, and T. E. Gill, "Environmental characterization of global sources of atmospheric soil dust identified with the Nimbus 7 Total Ozone Mapping Spectrometer (TOMS) absorbing aerosol product," *Reviews of Geophysics*, vol. 40, no. 1, p. 1002, 2002.

[8] S. Engelstaedter and R. Washington, "Temporal controls on global dust emissions: the role of surface gustiness," *Geophysical Research Letters*, vol. 34, no. 15, Article ID L15805, 2007.

[9] G. A. d'Almeida, P. Koepke, and E. P. Shettle, *Atmospheric Aerosol: Global Climatology and Radiative Characteristics*, A. Deepak, Hampton, Va, USA, 1991.

[10] J. M. Prospero, "Long-range transport of mineral dust in the global atmosphere: impact of African dust on the environment of the Southeastern United States," *Proceedings of the National Academy of Sciences of the United States of America*, vol. 96, no. 7, pp. 3396–3403, 1999.

[11] P. Forster, P. Artaxo, T. Berntsen et al., "Changes in atmospheric constituents and in radiative forcing," in *Climate Change 2007: The Physical Science Basis. Contribution of Working Group I to the Fourth Assessment Report of the Intergovernmental Panel on Climate Change*, S. Solomon, D. Qin, M. Manning et al., Eds., pp. 129–234, Cambridge University Press, New York, NY, USA, 2007.

[12] Z. Levin, E. Ganor, and V. Gladstein, "The effects of desert particles coated with sulfate on rain formation in the Eastern Mediterranean," *Journal of Applied Meteorology*, vol. 35, no. 9, pp. 1511–1523, 1996.

[13] R. L. Miller, I. Tegen, and J. Perlwitz, "Surface radiative forcing by soil dust aerosols and the hydrologic cycle," *Journal of Geophysical Research*, vol. 109, no. 4, p. D04203, 2004.

[14] Z. Levin, A. Teller, E. Ganor, and Y. Yin, "On the interactions of mineral dust, sea-salt particles, and clouds: a measurement

and modeling study from the Mediterranean Israeli Dust Experiment campaign," *Journal of Geophysical Research*, vol. 110, no. 20, p. D20202, 2005.

[15] D. Rosenfeld, "Suppression of rain and snow by urban and industrial air pollution," *Science*, vol. 287, no. 5459, pp. 1793–1796, 2000.

[16] H. R. Pruppacher and J. D. Klett, *Microphysics of Clouds and Precipitation*, Springer, New York, NY, USA, 1997.

[17] K. Sassen, P. J. DeMott, J. M. Prospero, and M. R. Poellot, "Saharan dust storms and indirect aerosol effects on clouds: CRYSTAL-FACE results," *Geophysical Research Letters*, vol. 30, no. 12, p. 1633, 2003.

[18] I. N. Sokolik, D. M. Winker, G. Bergametti et al., "Introduction to special section: outstanding problems in quantifying the radiative impacts of mineral dust," *Journal of Geophysical Research*, vol. 106, no. 16, pp. 18015–18027, 2001.

[19] I. N. Sokolik and O. B. Toon, "Direct radiative forcing by anthropogenic airborne mineral aerosols," *Nature*, vol. 381, no. 6584, pp. 681–683, 1996.

[20] WMO Secretariat, *WMO Sand and Dust Storm Warning Advisory and Assessment System (SDSWAS)—Science and Implementation Plan 2011–2015*, Research Department, Atmospheric Research and Environment Branch, 2011.

[21] K. T. Kanatani, I. Ito, W. K. Al-Delaimy et al., "Desert dust exposure is associated with increased risk of asthma hospitalization in children," *American Journal of Respiratory and Critical Care Medicine*, vol. 182, no. 12, pp. 1475–1481, 2010.

[22] H. H. Chang, R. D. Peng, and F. Dominici, "Estimating the acute health effects of coarse particulate matter accounting for exposure measurement error," *Biostatistics*, vol. 12, no. 4, pp. 637–652, 2011.

[23] R.-J. Zhang, K.-F. Ho, and Z.-X. Shen, "The role of aerosol in climate change, the environment, and human health," *Atmospheric and Oceanic Science Letters*, vol. 5, no. 2, pp. 156–161, 2012.

[24] C. Yoon, K. Ryu, J. Kim, K. Lee, and D. Park, "New approach for particulate exposure monitoring: determination of inhaled particulate mass by 24h real-time personal exposure monitoring," *Journal of Exposure Science and Environmental Epidemiology*, vol. 22, no. 4, pp. 344–351, 2012.

[25] WHO, *Meningococcal Meningitis Fact Sheet*, World Health Organization, Geneva, Switzerland, 2003.

[26] D. W. Griffin, "Atmospheric movement of microorganisms in clouds of desert dust and implications for human health," *Clinical Microbiology Reviews*, vol. 20, no. 3, pp. 459–477, 2007.

[27] P. N. Polymenakou, M. Mandalakis, E. G. Stephanou, and A. Tselepides, "Particle size distribution of airborne microorganisms and pathogens during an intense African dust event in the Eastern Mediterranean," *Environmental Health Perspectives*, vol. 116, no. 3, pp. 292–296, 2008.

[28] G. P. Gobbi, F. Barnaba, and L. Ammannato, "Estimating the impact of Saharan dust on the year 2001 PM_{10} record of Rome, Italy," *Atmospheric Environment*, vol. 41, no. 2, pp. 261–275, 2007.

[29] M. L. Sánchez, M. A. García, I. A. Pérez, and B. de Torre, "Ground laser remote sensing measurements of a Saharan dust outbreak in Central Spain. Influence on PM_{10} concentrations in the lower and upper Spanish plateaus," *Chemosphere*, vol. 67, no. 2, pp. 229–239, 2007.

[30] A. Pederzoli, M. Mircea, S. Finardi, A. di Sarra, and G. Zanini, "Quantification of Saharan dust contribution to PM_{10} concentrations over Italy during 2003–2005," *Atmospheric Environment*, vol. 44, no. 34, pp. 4181–4190, 2010.

[31] L. Perez, A. Tobias, X. Querol et al., "Coarse particles from Saharan dust and daily mortality," *Epidemiology*, vol. 19, no. 6, pp. 800–807, 2008.

[32] T. Aurelio, L. Perez, J. Díaz et al., "Short-term effects of particulate matter on total mortality during Saharan dust outbreaks: a case-crossover analysis in Madrid (Spain)," *Science of the Total Environment*, vol. 412-413, pp. 386–389, 2011.

[33] S. Mallone, M. Stafoggia, A. Faustini, G. P. Gobbi, A. Marconi, and F. Forastieri, "Saharan dust and associations between particulate matter and daily mortality in Rome, Italy," *Environmental Health Perspectives*, vol. 119, no. 10, pp. 1409–1414, 2011.

[34] S. Z. Sajani, R. Miglio, P. Bonasoni et al., "Saharan dust and daily mortality in Emilia-Romagna (Italy)," *Occupational and Environmental Medicine*, vol. 68, no. 6, pp. 446–451, 2011.

[35] T. Lekas, G. Kallos, J. Kushta, S. Solomos, and C. Spyrou, "Impacts of dust on aviation," in *Proceedings of the 6th International Workshop on Sand/Duststorms and Associated Dustfall*, Athens, Greece, September 2011.

[36] J. M. Prospero and T. N. Carlson, "Vertical and areal distribution of Saharan dust over the Western equatorial North Atlantic Ocean," *Journal of Geophysical Research*, vol. 77, no. 27, pp. 5255–5265, 1972.

[37] F. Dulac, P. Buat-Menard, D. Sutton, D. Tanré, G. Bergametti, and M. Desbois, "Assessment of the African airborne dust mass over the Western Mediterranean Sea using Meteosat data," *Journal of Geophysical Research*, vol. 97, no. 2, pp. 2489–2506, 1992.

[38] C. Moulin, C. E. Lambert, F. Dulac, and U. Dayan, "Control of atmospheric export of dust from North Africa by the North Atlantic Oscillation," *Nature*, vol. 387, no. 6634, pp. 691–694, 1997.

[39] C. Moulin, F. Dulac, C. E. Lambert et al., "Long-term daily monitoring of Saharan dust load over ocean using Meteosat ISCCP-B2 data 2. Accuracy of the method and validation using Sun photometer measurements," *Journal of Geophysical Research*, vol. 102, no. 14, pp. 16,959–16,969, 1997.

[40] R. B. Husar, J. M. Prospero, and L. L. Stowe, "Characterization of tropospheric aerosols over the oceans with the NOAA advanced very high resolution radiometer optical thickness operational product," *Journal of Geophysical Research*, vol. 102, no. 14, pp. 16,889–16,909, 1997.

[41] J. R. Herman, P. K. Bhartia, O. Torres, C. Hsu, C. Seftor, and E. Celarier, "Global distribution of UV-absorbing aerosols from Nimbus 7/TOMS data," *Journal of Geophysical Research*, vol. 102, no. 14, pp. 16,911–16,922, 1997.

[42] F. Barnaba and G. P. Gobbi, "Aerosol seasonal variability over the Mediterranean region and relative impact of maritime, continental and Saharan dust particles over the basin from MODIS data in the year 2001," *Atmospheric Chemistry and Physics*, vol. 4, no. 9-10, pp. 2367–2391, 2004.

[43] K. Schepanski, I. Tegen, B. Laurent, B. Heinold, and A. Macke, "A new Saharan dust source activation frequency map derived from MSG-SEVIRI IR-channels," *Geophysical Research Letters*, vol. 34, no. 18, p. L18803, 2007.

[44] E. Carboni, G. E. Thomas, A. M. Sayer et al., "Desert dust satellite retrieval intercomparison," *Atmospheric Measurement Techiques*, vol. 5, pp. 691–746, 2012.

[45] G. Fiocco and L. D. Smullin, "Detection of scattering layers in the upper atmosphere (60–140 km) by optical radar," *Nature*, vol. 199, no. 4900, pp. 1275–1276, 1963.

[46] A. Ansmann, M. Riebesell, and C. Weitkamp, "Measurement of atmospheric aerosol extinction profiles with a Raman lidar," *Optics Letters*, vol. 15, no. 13, pp. 746–748, 1990.

[47] A. Ansmann, M. Riebesell, U. Wandinger et al., "Combined Raman elastic-backscatter lidar for vertical profiling of moisture, aerosol extinction, backscatter and lidar ratio," *Applied Physics B*, vol. 55, no. 1, pp. 18–28, 1992.

[48] D. N. Whiteman, S. H. Melfi, and R. A. Ferrare, "Raman lidar system for the measurement of water vapor and aerosols in the Earth's atmosphere," *Applied Optics*, vol. 31, no. 16, pp. 3068–3082, 1992.

[49] J. T. Sroga, E. W. Eloranta, S. T. Shipley, F. L. Roesler, and P. J. Tryon, "High spectral resolution lidar to measure optical scattering properties of atmospheric aerosols. 2: calibration and data analysis," *Applied Optics*, vol. 22, no. 23, pp. 3725–3732, 1983.

[50] P. B. Russell and J. M. Livingston, "Slant-lidar aerosol extinction measurements and their relation to measured and calculated albedo changes," *Journal of Applied Meteorology*, vol. 23, no. 8, pp. 1204–1221, 1984.

[51] J. D. Klett, "Lidar calibration and extinction coefficients," *Applied Optics*, vol. 22, no. 4, pp. 514–515, 1983.

[52] F. G. Fernald, "Analysis of atmospheric lidar observations: some comments," *Applied Optics*, vol. 23, no. 5, pp. 652–653, 1984.

[53] J. D. Klett, "Lidar inversion with variable backscatter/extinction ratios," *Applied Optics*, vol. 24, no. 11, pp. 1638–1643, 1985.

[54] J. D. Klett, "Extinction boundary value algorithms for lidar inversion," *Applied Optics*, vol. 25, no. 15, pp. 2462–2464, 1986.

[55] S. T. Shipley, D. H. Tracy, E. W. Eloranta et al., "High spectral resolution lidar to measure optical scattering properties of atmospheric aerosols. 1: theory and instrumentation," *Applied Optics*, vol. 22, no. 23, pp. 3716–3724, 1983.

[56] M. Kano, "On the determination of backscattering and extinction coefficient of the atmosphere by using a laser radar," *Papers Meteorological Geophysics*, vol. 19, no. 1, pp. 121–129, 1968.

[57] P. M. Hamilton, "Lidar measurement of backscatter and attenuation of atmospheric aerosol," *Atmospheric Environment*, vol. 3, no. 2, pp. 221–223, 1969.

[58] V. M. Karyampudi, S. P. Palm, J. A. Reagen et al., "Validation of the Saharan dust plume conceptual model using lidar, meteosat, and ECMWF data," *Bulletin of the American Meteorological Society*, vol. 80, no. 6, pp. 1045–1075, 1999.

[59] M. A. Vaughan, Z. Liu, and A. H. Omar, "Multi-wavelength analysis of a lofted aerosol layer measured by LITE," in *Proceedings of the 22nd International Laser Radar Conference*, pp. 495–499, European Space Agency, Matera, Italy, July 2004.

[60] W. D. Hart, J. D. Spinhirne, S. P. Palm, and D. L. Hlavka, "Height distribution between cloud and aerosol layers from the GLAS spaceborne lidar in the Indian Ocean region," *Geophysical Research Letters*, vol. 32, no. 22, p. L22S06, 2005.

[61] J. Bösenberg and V. Matthias, "EARLINET: a European aerosol research lidar network to establish an aerosol climatology," MPI-Report 348, Hamburg, Germany, 2003.

[62] T. Murayama, N. Sugimoto, I. Uno et al., "Ground-based network observation of Asian dust events of April 1998 in East Asia," *Journal of Geophysical Research*, vol. 106, no. 16, pp. 18,345–18,359, 2001.

[63] E. J. Welton, J. R. Campbell, J. D. Spinhirne, and V. S. Scott, "Global monitoring of clouds and aerosols using a network of micro-pulse lidar systems," in *Lidar Remote Sensing for Industry and Environment Monitoring*, U. N. Singh, T. Itabe, and N. Sugimoto, Eds., vol. 4153 of *Proceedings of SPIE*, pp. 151–158, Sendai, Japan, October 2000.

[64] GAW, "Plan for the implementation of the GAW aerosol lidar observation network GALION," GAW Report 178, Hamburg, Germany, 2007.

[65] B. Heese, H. Flentje, D. Althausen, A. Ansmann, and S. Frey, "Ceilometer lidar comparison: backscatter coefficient retrieval and signal-to-noise ratio determination," *Atmospheric Measurement Techniques*, vol. 3, pp. 1763–1770, 2010.

[66] D. M. Winker, W. H. Hunt, and M. J. McGill, "Initial performance assessment of CALIOP," *Geophysical Research Letters*, vol. 34, no. 19, Article ID L19803, 2007.

[67] J. S. Reid, J. E. Kinney, D. L. Westphal et al., "Analysis of measurements of Saharan dust by airborne and ground-based remote sensing methods during the Puerto Rico Dust Experiment (PRIDE)," *Journal of Geophysical Research*, vol. 108, no. 19, p. 8586, 2003.

[68] J.-F. Léon, D. Tanré, J. Pelon, Y. J. Kaufman, J. M. Haywood, and B. Chatenet, "Profiling of a Saharan dust outbreak based on a synergy between active and passive remote sensing," *Journal of Geophysical Research*, vol. 108, no. 18, p. 8575, 2003.

[69] D. Müller, K. Franke, A. Ansmann, D. Althausen, and F. Wagner, "Indo-Asian pollution during INDOEX: microphysical particle properties and single-scattering albedo inferred from multiwavelength lidar observations," *Journal of Geophysical Research*, vol. 108, no. 19, p. 4600, 2003.

[70] B. J. Johnson, J. Pelon, P. Formenti, and J. Haywood, "Aerosol studies during AMMA," *CLIVAR Exchanges*, vol. 41, no. 12(2), pp. 9–11, 2007.

[71] J. Cuesta, D. Edouart, M. Mimouni et al., "Multiplatform observations of the seasonal evolution of the Saharan atmospheric boundary layer in Tamanrasset, Algeria, in the framework of the African Monsoon Multidisciplinary Analysis field campaign conducted in 2006," *Journal of Geophysical Research*, vol. 113, p. D00C07, 2008.

[72] B. T. Johnson, B. Heese, S. A. McFarlane, P. Chazette, A. Jones, and N. Bellouin, "Vertical distribution and radiative effects of mineral dust and biomass burning aerosol over West Africa during DABEX," *Journal of Geophysical Research*, vol. 113, p. D00C12, 2008.

[73] B. Heese and M. Wiegner, "Vertical aerosol profiles from Raman polarization lidar observations during the dry season AMMA field campaign," *Journal of Geophysical Research*, vol. 113, p. D00C11, 2008.

[74] Y. Hara, K. Yumimoto, I. Uno et al., "Asian dust outflow in the PBL and free atmosphere retrieved by NASA CALIPSO and an assimilated dust transport model," *Atmospheric Chemistry and Physics*, vol. 9, no. 4, pp. 1227–1239, 2009.

[75] L. Mona, A. Amodeo, G. D'Amico, A. Giunta, F. Madonna, and G. Pappalardo, "Multi-wavelength Raman lidar observations of the Eyjafjallajökull volcanic cloud over Potenza, Southern Italy," *Atmospheric Chemistry and Physics*, vol. 12, pp. 2229–2244, 2012.

[76] E. J. Welton, K. J. Voss, P. K. Quinn et al., "Measurements of aerosol vertical profiles and optical properties during INDOEX 1999 using micropulse lidars," *Journal of Geophysical Research*, vol. 107, p. 8019, 2002.

[77] A. Ansmann, J. Bösenberg, A. Chiakovsky et al., "Long-range transport of Saharan dust to Northern Europe: the 11–16 October 2001 outbreak observed with EARLINET," *Journal of Geophysical Research*, vol. 108, no. 24, p. 4783, 2003.

[78] A. Shimizu, N. Sugimoto, I. Matsui et al., "Continuous observations of Asian dust and other aerosols by polarization lidars in China and Japan during ACE-Asia," *Journal of Geophysical Research*, vol. 109, p. D19S17, 2004.

[79] A. Papayannis, V. Amiridis, L. Mona et al., "Systematic lidar observations of Saharan dust over Europe in the frame of EARLINET (2000–2002)," *Journal of Geophysical Research*, vol. 113, p. D10204, 2008.

[80] Z. Liu, A. Omar, M. Vaughan et al., "CALIPSO lidar observations of the optical properties of Saharan dust: a case study of long-range transport," *Journal of Geophysical Research*, vol. 113, p. D07207, 2008.

[81] Y. Ben-Ami, I. Koren, and O. Altaratz, "Patterns of Saharan dust transport over the Atlantic: Winter vs. Summer, based on CALIPSO first year data," *Atmospheric Chemistry and Physics*, vol. 9, pp. 7867–7875, 2009.

[82] C. M. R. Platt, "Lidar and radiometric observations of cirrus clouds," *Journal of Atmospheric Science*, vol. 30, no. 6, pp. 1191–1204, 1973.

[83] S. A. Young, "Analysis of lidar backscatter profiles in optically thin clouds," *Applied Optics*, vol. 34, no. 30, pp. 7019–7031, 1995.

[84] J. R. Campbell, D. L. Hlavka, E. J. Welton et al., "Full-time, eye-safe cloud and aerosol lidar observation at atmospheric radiation measurement program sites: instruments and data processing," *Journal of Atmospheric and Oceanic Technology*, vol. 19, no. 4, pp. 431–442, 2002.

[85] T. Sakai, T. Nagai, M. Nakazato, Y. Mano, and T. Matsumura, "Ice clouds and Asian dust studied with lidar measurements of particle extinction-to-backscatter ratio, particle depolarization, and water-vapor mixing ratio over Tsukuba," *Applied Optics*, vol. 42, no. 36, pp. 7103–7116, 2003.

[86] G. P. Gobbi, F. Barnaba, and L. Ammannato, "The vertical distribution of aerosols, Saharan dust and cirrus clouds in Rome (Italy) in the year 2001," *Atmospheric Chemistry and Physics*, vol. 4, no. 2, pp. 351–359, 2004.

[87] W. Su, G. L. Schuster, N. G. Loeb et al., "Aerosol and cloud interaction observed from high spectral resolution lidar data," *Journal of Geophysical Research*, vol. 113, p. D24202, 2008.

[88] M. A. Vaughan, K. A. Powell, R. E. Kuehn et al., "Fully automated detection of cloud and aerosol layers in the CALIPSO lidar measurements," *Journal of Atmospheric and Oceanic Technology*, vol. 26, no. 10, pp. 2034–2050, 2009.

[89] D. Josset, J. Pelon, A. Garnier et al., "Cirrus optical depth and lidar ratio retrieval from combined CALIPSO-CloudSat observations using ocean surface echo," *Journal of Geophysical Research*, vol. 117, p. D05207, 2012.

[90] G. Feingold, W. L. Eberhard, D. E. Veron, and M. Previdi, "First measurements of the Twomey indirect effect using ground-based remote sensors," *Geophysical Research Letters*, vol. 30, no. 6, p. 1287, 2003.

[91] G. M. McFarquhar, S. Ghan, J. Verlinde et al., "Indirect and semi-direct aerosol campaign: the impact of Arctic aerosols on clouds," *Bulletin of the American Meteorological Society*, vol. 92, no. 2, pp. 183–201, 2011.

[92] M. J. McGill, L. Li, W. D. Hart et al., "Combined lidar-radar remote sensing: initial results from CRYSTAL-FACE," *Journal of Geophysical Research*, vol. 109, p. D07203, 2004.

[93] J. Bösenberg, "Ground-based differential absorption lidar for water-vapor and temperature profiling: methodology," *Applied Optics*, vol. 37, no. 18, pp. 3845–3860, 1998.

[94] J. E. M. Goldsmith, F. H. Blair, S. E. Bisson et al., "Turn-key Raman lidar for profiling atmospheric water vapor, clouds, and aerosols," *Applied Optics*, vol. 37, no. 21, pp. 4979–4990, 1998.

[95] A. Behrendt, T. Nakamura, and T. Tsuda, "Combined temperature lidar for measurements in the troposphere, stratosphere, and mesosphere," *Applied Optics*, vol. 43, no. 14, pp. 2930–2939, 2004.

[96] P. Keckhut, S. McDermid, D. Swart et al., "Review of ozone and temperature lidar validations performed within the framework of the Network for the Detection of Stratospheric Change," *Journal of Environmental Monitoring*, vol. 6, no. 9, pp. 721–733, 2004.

[97] E. W. Eloranta, J. M. King, and J. A. Weinman, "The determination of wind speeds in the boundary layer by monostatic lidar," *Journal of Applied Meteorology*, vol. 14, no. 8, pp. 1485–1489, 1975.

[98] A. Stoffelen, J. Pailleux, E. Källén et al., "The atmospheric dynamics mission for global wind field measurement," *Bulletin of the American Meteorological Society*, vol. 86, no. 1, pp. 73–87, 2005.

[99] P. I. Richter, "Air pollution monitoring with LIDAR," *TrAC Trends in Analytical Chemistry*, vol. 13, no. 7, pp. 267–275, 1994.

[100] M. J. T. Milton, P. T. Woods, B. W. Jolliffe, N. R. W. Swann, and T. J. McIlveen, "Measurements of toluene and other aromatic hydrocarbons by differential-absorption LIDAR in the near-ultraviolet," *Applied Physics B*, vol. 55, no. 1, pp. 41–45, 1992.

[101] K. Sassen, "The polarization lidar technique for cloud research: a review and current assessment," *Bulletin of American Meteorological Society*, vol. 72, no. 12, pp. 1848–1866, 1991.

[102] V. Wulfmeyer, C. Flamant, A. Behrendt et al., "Advances in the understanding of convective processes and precipitation over low-mountain regions through the Convective and Orographically-induced Precipitation Study (COPS)," *Quarterly Journal of the Royal Meteorological Society*, vol. 137, no. 1, pp. 1–2, 2011.

[103] I. Mattis, D. Müller, A. Ansmann et al., "Ten years of multiwavelength Raman lidar observations of free-tropospheric aerosol layers over central Europe: geometrical properties and annual cycle," *Journal of Geophysical Research*, vol. 113, p. D20202, 2008.

[104] V. Amiridis, D. S. Balis, E. Giannakaki et al., "Optical characteristics of biomass burning aerosols over Southeastern Europe determined from UV-Raman lidar measurements," *Atmospheric Chemistry and Physics*, vol. 9, no. 7, pp. 2431–2440, 2009.

[105] A. H. Omar, D. M. Winker, M. A. Vaughan et al., "The CALIPSO automated aerosol classification and lidar ratio selection algorithm," *Journal of Atmospheric and Oceanic Technology*, vol. 26, no. 10, pp. 1994–2014, 2009.

[106] C. Weitkamp, *Lidar: Range-Resolved Optical Remote Sensing of the Atmosphere*, vol. 102 of *Springer Series in Optical Sciences*, 2005.

[107] J. D. Klett, "Stable analytical inversion solution for processing lidar returns," *Applied Optics*, vol. 20, no. 2, pp. 211–220, 1981.

[108] A. Amodeo, "Uncertainties evaluation for aerosol optical properties," in *Proceedings of the 2nd GALION Workshop—EARLINET-ASOS Symposium*, Geneva, Switzerland, September 2010, http://alg.umbc.edu/galion.

[109] B. T. N. Evans, "Sensitivity of the backscatter/extinction ratio to changes in aerosol properties: implications for lidar," *Applied Optics*, vol. 27, no. 15, pp. 3299–3305, 1988.

[110] M. I. Mishchenko, L. D. Travis, R. A. Kahn, and R. A. West, "Modeling phase functions for dustlike tropospheric aerosols using a shape mixture of randomly oriented polydisperse spheroids," *Journal of Geophysical Research*, vol. 102, no. 14, pp. 16,831–16,847, 1997.

[111] J. Ackermann, "The extinction-to-backscatter ratio of tropospheric aerosol: a numerical study," *Journal of Atmospheric and Oceanic Technology*, vol. 15, no. 4, pp. 1043–1050, 1998.

[112] E. J. Welton, K. J. Voss, H. R. Gordon et al., "Ground-based lidar measurements of aerosols during ACE-2: instrument description, results, and comparisons with other ground-based and airborne measurements," *Tellus B*, vol. 52, no. 2, pp. 636–651, 2000.

[113] U. Wandinger and A. Ansmann, "Experimental determination of the lidar overlap profile with Raman lidar," *Applied Optics*, vol. 41, no. 3, pp. 511–514, 2002.

[114] S. W. Dho, Y. J. Park, and H. J. Kong, "Experimental determination of a geometric form factor in a lidar equation for an inhomogeneous atmosphere," *Applied Optics*, vol. 36, no. 24, pp. 6009–6010, 1997.

[115] F. Barnaba and G. P. Gobbi, "Lidar estimation of tropospheric aerosol extinction, surface area and volume: maritime and desert-dust cases," *Journal of Geophysical Research*, vol. 106, no. 3, pp. 3005–3018, 2001.

[116] F. Barnaba and G. P. Gobbi, "Modeling the aerosol extinction versus backscatter relationship for lidar applications: maritime and continental conditions," *Journal of Atmospheric and Oceanic Technology*, vol. 21, no. 3, pp. 428–442, 2004.

[117] J. Cuesta, P. H. Flamant, and C. Flamant, "Synergetic technique combining elastic backscatter lidar data and sunphotometer AERONET inversion for retrieval by layer of aerosol optical and microphysical properties," *Applied Optics*, vol. 47, no. 25, pp. 4598–4611, 2008.

[118] T. L. Anderson, S. J. Masonis, D. S. Covert, R. J. Charlson, and M. J. Rood, "In situ measurement of the aerosol extinction-to-backscatter ratio at a polluted continental site," *Journal of Geophysical Research*, vol. 105, no. 22, pp. 26907–26915, 2000.

[119] C. Cattrall, J. Reagan, K. Thome, and O. Dubovik, "Variability of aerosol and spectral lidar and backscatter and extinction ratios of key aerosol types derived from selected Aerosol Robotic Network locations," *Journal of Geophysical Research*, vol. 110, p. D10S11, 2005.

[120] D. Müller, A. Ansmann, I. Mattis et al., "Aerosol-type-dependent lidar ratios observed with Raman lidar," *Journal of Geophysical Research*, vol. 112, p. D16202, 2007.

[121] I. Mattis, A. Ansmann, D. Müller, U. Wandinger, and D. Althausen, "Multilayer aerosol observations with dual-wavelength Raman lidar in the framework of EARLINET," *Journal of Geophysical Research*, vol. 109, p. D13203, 2004.

[122] A. Papayannis, D. Balis, V. Amiridis et al., "Measurements of Saharan dust aerosols over the Eastern Mediterranean using elastic backscatter-Raman lidar, spectrophotometric and satellite observations in the frame of the EARLINET project," *Atmospheric Chemistry and Physics*, vol. 5, no. 8, pp. 2065–2079, 2005.

[123] L. Mona, A. Amodeo, M. Pandolfi, and G. Pappalardo, "Saharan dust intrusions in the Mediterranean area: three years of Raman lidar measurements," *Journal of Geophysical Research*, vol. 111, p. D16203, 2006.

[124] H. Flentje, H. Claude, T. Elste et al., "The Eyjafjallajökull eruption in April 2010—detection of volcanic plume using in-situ measurements, ozone sondes and lidar-ceilometer profiles," *Atmospheric Chemistry and Physics*, vol. 10, no. 20, pp. 10085–10092, 2010.

[125] M. Wiegner, "Potential of ceilometers for aerosol remote sensing: a preliminary assessment," in *Proceedings of the 25th International Laser Radar Conference*, July 2010.

[126] I. Binietoglou, A. Amodeo, G. D'Amico et al., "Examination of possible synergy between lidar and ceilometer for the monitoring of atmospheric aerosols," in *Lidar Technology, Techniques, and Measurements for Atmospheric Remote Sensing VII*, U. N. Singh and G. Pappalardo, Eds., vol. 8182 of *Proceedings of SPIE*, SPIE, Bellingham, Wash, USA, 2011.

[127] G. Tsaknakis, A. Papayannis, P. Kokkalis et al., "Inter-comparison of lidar and ceilometer retrievals for aerosol and Planetary Boundary Layer profiling over Athens, Greece," *Atmospheric Measurement Techniques*, vol. 4, pp. 1261–1273, 2011.

[128] M. Haeffelin, F. Angelini, Y. Morille et al., "Evaluation of mixing-height retrievals from automatic profiling lidars and ceilometers in view of future integrated networks in Europe," *Boundary-Layer Meteorology*, vol. 143, no. 1, pp. 49–75, 2011.

[129] M. Adam, V. A. Kovalev, C. Wold et al., "Application of the Kano-Hamilton multiangle inversion method in clear atmospheres," *Journal of Atmospheric and Oceanic Technology*, vol. 24, no. 12, pp. 2014–2028, 2007.

[130] V. Kovalev, C. Wold, A. Petkov, and W. M. Hao, "Modified technique for processing multiangle lidar data measured in clear and moderately polluted atmospheres," *Applied Optics*, vol. 50, no. 25, pp. 4957–4966, 2011.

[131] D. N. Whiteman, "Examination of the traditional Raman lidar technique. II. Evaluating the ratios for water vapor and aerosols," *Applied Optics*, vol. 42, no. 15, pp. 2593–2608, 2003.

[132] R. Ferrare, D. Turner, M. Clayton et al., "Evaluation of daytime measurements of aerosols and water vapor made by an operational Raman lidar over the Southern Great Plains," *Journal of Geophysical Research*, vol. 111, p. D05S08, 2006.

[133] G. Pappalardo, A. Amodeo, L. Mona, M. Pandolfi, N. Pergola, and V. Cuomo, "Raman lidar observations of aerosol emitted during the 2002 Etna eruption," *Geophysical Research Letters*, vol. 31, L05120 pages, 2004.

[134] M. G. Villani, L. Mona, A. Maurizi et al., "Transport of volcanic aerosol in the troposphere: the case study of the 2002 Etna plume," *Journal of Geophysical Research*, vol. 111, p. D21102, 2006.

[135] J. W. Hair, C. A. Hostetler, A. L. Cook et al., "Airborne high spectral resolution lidar for profiling aerosol optical properties," *Applied Optics*, vol. 47, no. 36, pp. 6734–6753, 2008.

[136] European Space Agency (ESA), "Earth clouds, aerosols, and radiation explorer," ESA Technical Report SP–1279(1), ESTEC, Noorwijk, The Netherlands, 2004.

[137] D. Müller, U. Wandinger, and A. Ansmann, "Microphysical particle parameters from extinction and backscatter lidar data by inversion with regularization: simulation," *Applied Optics*, vol. 38, no. 12, pp. 2358–2368, 1999.

[138] C. Böckmann, I. Mironova, D. Müller, L. Schneidenbach, and R. Nessler, "Microphysical aerosol parameters from multi-wavelength lidar," *Journal of the Optical Society of America A*, vol. 22, no. 3, pp. 518–528, 2005.

[139] I. Veselovskii, A. Kolgotin, D. Müller, and D. N. Whiteman, "Information content of multiwavelength lidar data with respect to microphysical particle properties derived from eigenvalue analysis," *Applied Optics*, vol. 44, no. 25, pp. 5292–5303, 2005.

[140] D. Müller, I. Mattis, U. Wandinger, A. Ansmann, D. Althausen, and A. Stohl, "Raman lidar observations of aged Siberian and Canadian forest fire smoke in the free troposphere over Germany in 2003: microphysical particle characterization," *Journal of Geophysical Research*, vol. 110, p. D17201, 2005.

[141] A. Chaikovsky, S. Denisov, J. Grudo et al., "Combined lidar/sun-radiometer remote sensing technique for studying long range aerosol transport," in *Proceedings of Saudi International Electronics, Communications and Photonics Conference (SIECPC '11)*, pp. 1–5, IEEE, Riyadh, Saudi Arabia, April 2011.

[142] A. P. Chaikovsky, O. Dubovik, B. N. Holben, and A. I. Bril, "Methodology to retrieve atmospheric aerosol parameters by combining ground-based measurements of multiwavelength lidar and sun sky scanning radiometer," in *Proceedings of the 8th Internationla Symposium on Atmospheric and Ocean Optics: Atmospheric Physics*, G. A. Zherebtsov, G. G. Matvienko, V. A. Banakh et al., Eds., vol. 4678 of *Proceedings of SPIE*, pp. 257–268, Irkutsk, Russia, June 2001.

[143] V. Freudenthaler, M. Esselborn, M. Wiegner et al., "Depolarization ratio profiling at several wavelengths in pure Saharan dust during SAMUM 2006," *Tellus B*, vol. 61, no. 1, pp. 165–179, 2009.

[144] B. Tatarov and N. Sugimoto, "Estimation of quartz concentration in the tropospheric mineral aerosols using combined Raman and high-spectral-resolution lidars," *Optics Letters*, vol. 30, no. 24, pp. 3407–3409, 2005.

[145] D. Müller, I. Mattis, B. Tatarov et al., "Mineral quartz concentration measurements of mixed mineral dust/urban haze pollution plumes over Korea with multiwavelength aerosol Raman-quartz lidar," *Geophysical Research Letters*, vol. 37, L20810 pages, 2010.

[146] B. Tatarov, D. Müller, D. H. Shin et al., "Lidar measurements of Raman scattering at ultraviolet wavelength from mineral dust over East Asia," *Optics Express*, vol. 19, no. 2, pp. 1569–1581, 2011.

[147] D. G. Steyn, M. Baldi, and R. M. Hoff, "The detection of mixed layer depth and entrainment zone thickness from lidar backscatter profiles," *Journal of Atmospheric and Oceanic Technology*, vol. 16, no. 7, pp. 953–959, 1999.

[148] Y. Morille, M. Haeffelin, P. Drobinski, and J. Pelon, "STRAT: an automated algorithm to retrieve the vertical structure of the atmosphere from single-channel lidar data," *Journal of Atmospheric and Oceanic Technology*, vol. 24, no. 5, pp. 761–775, 2007.

[149] L. Wang and K. Sassen, "Wavelet analysis of cirrus multiscale structures from lidar backscattering: a cirrus uncinus complex case study," *Journal of Applied Meteorology and Climatology*, vol. 47, no. 10, pp. 2645–2658, 2008.

[150] P. Di Girolamo, G. Pappalardo, V. Berardi et al., "Lidar observations of the stratospheric aerosol layer over Southern Italy in the period 1991–1995," *Journal of Geophysical Research*, vol. 101, no. 13, pp. 18,765–18,773, 1996.

[151] I. Veselovskii, O. Dubovik, A. Kolgotin et al., "Application of randomly oriented spheroids for retrieval of dust particle parameters from multiwavelength lidar measurements," *Journal of Geophysical Research*, vol. 115, p. D21203, 2010.

[152] I. Veselovskii, A. Kolgotin, V. Griaznov, D. Müller, U. Wandinger, and D. N. Whiteman, "Inversion with regularization for the retrieval of tropospheric aerosol parameters from multiwavelength lidar sounding," *Applied Optics*, vol. 41, no. 18, pp. 3685–3699, 2002.

[153] M. Tesche, A. Ansmann, D. Müller et al., "Vertical profiling of Saharan dust with Raman lidars and airborne HSRL in Southern Morocco during SAMUM," *Tellus B*, vol. 61, no. 1, pp. 144–164, 2009.

[154] M. Tesche, S. Gross, A. Ansmann et al., "Profiling of Saharan dust and biomass-burning smoke with multiwavelength polarization Raman lidar at Cape Verde," *Tellus B*, vol. 63, no. 4, pp. 649–676, 2011.

[155] S. Groß, M. Tesche, V. Freudenthaler et al., "Characterization of Saharan dust, marine aerosols and mixtures of biomass-burning aerosols and dust by means of multi-wavelength depolarization and Raman lidar measurements during SAMUM 2," *Tellus B*, vol. 63, no. 4, pp. 706–724, 2011.

[156] Veselovskii et al., "Vertical profiles of dust particle size inferred from inversion of multiwavelength Raman lidar observations and comparison toairborne in-situ measurements," submitted to. *Applied Optics*.

[157] E. Hamonou, P. Chazette, D. Balis et al., "Characterization of the vertical structure of Saharan dust export to the Mediterranean basin," *Journal of Geophysical Research*, vol. 104, no. 18, pp. 22257–22270, 1999.

[158] V. Ramanathan, P. J. Crutzen, J. Lelieveld et al., "Indian Ocean Experiment: an integrated analysis of the climate forcing and effects of the great Indo-Asian haze," *Journal of Geophysical Research*, vol. 106, no. 22, pp. 28,371–28,398, 2001.

[159] H. Maring, D. L. Savoie, M. A. Izaguirre, L. Custals, and J. S. Reid, "Mineral dust aerosol size distribution change during atmospheric transport," *Journal of Geophysical Research*, vol. 108, p. 8592, 2003.

[160] J. S. Reid and H. B. Maring, "Foreword to special section on the Puerto Rico Dust Experiment (PRIDE)," *Journal of Geophysical Research*, vol. 108, no. 19, p. 8585, 2003.

[161] S. A. Christopher, J. Wang, Q. Ji, and S. C. Tsay, "Estimation of diurnal shortwave dust aerosol radiative forcing during PRIDE," *Journal of Geophysical Research*, vol. 108, no. 19, p. 8596, 2003.

[162] D. Tanré, J. Haywood, J. Pelon et al., "Measurement and modeling of the Saharan dust radiative impact: overview of the Saharan Dust Experiment (SHADE)," *Journal of Geophysical Research*, vol. 108, no. 18, p. 8574, 2003.

[163] J. H. Seinfeld, G. R. Carmichael, R. Arimoto et al., "ACE-ASIA: regional climatic and atmospheric chemical effects of Asian dust and pollution," *Bulletin of the American Meteorological Society*, vol. 85, no. 3, pp. 367–380, 2004.

[164] N. Sugimoto, I. Uno, M. Nishikawa et al., "Record heavy Asian dust in Beijing in 2002: observations and model analysis of recent events," *Geophysical Research Letters*, vol. 30, p. 1640, 2003.

[165] G. P. Gobbi, F. Barnaba, R. Van Dingenen, J. P. Putaud, M. Mircea, and M. C. Facchini, "Lidar and in situ observations of continental and Saharan aerosol: closure analysis of particles optical and physical properties," *Atmospheric Chemistry and Physics*, vol. 3, no. 6, pp. 2161–2172, 2003.

[166] P. J. DeMott, K. Sassen, M. R. Poellot et al., "African dust aerosols as atmospheric ice nuclei," *Geophysical Research Letters*, vol. 30, no. 14, p. 1732, 2003.

[167] F. Immler and O. Schrems, "Vertical profiles, optical and microphysical properties of Saharan dust layers determined by a ship-borne lidar," *Atmospheric Chemistry and Physics*, vol. 3, no. 5, pp. 1353–1364, 2003.

[168] T. F. Eck, B. N. Holben, J. S. Reid et al., "Spatial and temporal variability of column-integrated aerosol optical properties in the Southern Arabian Gulf and United Arab Emirates in Summer," *Journal of Geophysical Research*, vol. 113, p. D01204, 2008.

[169] R. A. Hansell, K. N. Liou, S. C. Ou, S. C. Tsay, Q. Ji, and J. S. Reid, "Remote sensing of mineral dust aerosol using AERI during the UAE2: a modeling and sensitivty study," *Journal of Geophysical Research*, vol. 113, p. D18202, 2008.

[170] J.-L. Redelsperger, C. D. Thorncroft, A. Diedhiou, T. Lebel, D. J. Parker, and J. Polcher, "African monsoon multidisciplinary analysis: an international research project and field campaign," *Bulletin of the American Meteorological Society*, vol. 87, no. 12, pp. 1739–1746, 2006.

[171] J. M. Haywood, J. Pelon, P. Formenti et al., "Overview of the dust and biomass-burning experiment and African monsoon multidisciplinary analysis special observing period-0," *Journal of Geophysical Research*, vol. 113, p. D00C17, 2008.

[172] C. L. McConnell, E. J. Highwood, H. Coe et al., "Seasonal variations of the physical and optical characteristics of Saharan dust: results from the Dust Outflow and Deposition to the Ocean (DODO) experiment," *Journal of Geophysical Research*, vol. 113, no. 14, p. D14S05, 2008.

[173] M. Mikami, G. Y. Shi, S. Yabuki et al., "Aeolian dust experiment on climate impact: an overview of Japan-China joint project ADEC," *Global and Planetary Change*, vol. 52, no. 1–4, pp. 142–172, 2006.

[174] E. Nowottnick, P. Colarco, A. da Silva, D. Hlavka, and M. McGill, "The fate of Saharan dust across the Atlantic and implications for a central American dust barrier," *Atmospheric Chemistry and Physics*, vol. 11, pp. 8415–8431, 2011.

[175] A. Ansmann, A. Petzold, K. Kandler et al., "Saharan mineral dust experiments SAMUM-1 and SAMUM-2: what have we learned?" *Tellus*, vol. 63, no. 4, pp. 403–429, 2011.

[176] B. Weinzierl, D. Sauer, M. Esselborn et al., "Microphysical and optical properties of dust and tropical biomass burning aerosol layers in the Cape Verde region—an overview of the airborne in situ and lidar measurements during SAMUM-2," *Tellus*, vol. 63, no. 4, pp. 589–618, 2011.

[177] O. Torres, H. Jethva, and C. Ahn, "Long range transport of Saharan Dust: the April 2011 dust storm over Western Europe," in *Proceedings of the 6th International Workshop on Sand/Dust Storms and Associated Dustfall*, Athens, Greece, September 2011.

[178] R. A. Ferrare, D. D. Turner, L. H. Brasseur, W. F. Feltz, O. Dubovik, and T. P. Tooman, "Raman lidar measurements of the aerosol extinction-to-backscatter ratio over the Southern Great Plains," *Journal of Geophysical Research*, vol. 106, no. 17, pp. 20,333–20,347, 2001.

[179] H. A. McGowan and J. Soderholm, "Laser ceilometer measurements of Australian dust storm highlight need for reassessment of atmospheric dust plume loads," *Geophysical Research Letters*, vol. 39, p. L02804, 2012.

[180] B. N. Holben, T. F. Eck, I. Slutsker et al., "AERONET—a federated instrument network and data archive for aerosol characterization," *Remote Sensing of Environment*, vol. 66, no. 1, pp. 1–16, 1998.

[181] S. Basart, C. Pérez, E. Cuevas, J. M. Baldasano, and G. P. Gobbi, "Aerosol characterization in Northern Africa, Northeastern Atlantic, Mediterranean basin and Middle East from direct-sun AERONET observations," *Atmospheric Chemistry and Physics*, vol. 9, no. 21, pp. 8265–8282, 2009.

[182] A. di Sarra, M. Cacciani, P. Chamard et al., "Effects of desert dust and ozone on the ultraviolet irradiance at the Mediterranean island of Lampedusa during PAUR II," *Journal of Geophysical Research*, vol. 107, no. 18, p. 8135, 2002.

[183] F. Dulac and P. Chazette, "Airborne study of a multi-layer aerosol structure in the Eastern Mediterranean observed with the airborne polarized lidar ALEX during a STAAARTE campaign (7 June 1997)," *Atmospheric Chemistry and Physics*, vol. 3, no. 5, pp. 1817–1831, 2003.

[184] A. M. Tafuro, F. Barnaba, F. De Tomasi, M. R. Perrone, and G. P. Gobbi, "Saharan dust particle properties over the central Mediterranean," *Atmospheric Research*, vol. 81, no. 1, pp. 67–93, 2006.

[185] F. A. Vishkaee, C. Flamant, J. Cuesta, P. Flamant, and H. R. Khalesifard, "Multiplatform observations of dust vertical distribution during transport over Northwest Iran in the Summertime," *Journal of Geophysical Research*, vol. 116, p. D05206, 2011.

[186] A. di Sarra, T. di Iorio, M. Cacciani, G. Fiocco, and D. Fuà, "Saharan dust profiles measured by lidar at Lampedusa," *Journal of Geophysical Research*, vol. 106, no. 10, pp. 10,335–10,347, 2001.

[187] T. di Iorio, A. di Sarra, D. M. Sferlazzo et al., "Seasonal evolution of the tropospheric aerosol vertical profile in the central Mediterranean and role of desert dust," *Journal of Geophysical Research*, vol. 114, p. D02201, 2009.

[188] P. Chazette, J. Pelon, C. Moulin et al., "Lidar and satellite retrieval of dust aerosols over the Azores during SOFIA/ASTEX," *Atmospheric Environment*, vol. 35, no. 25, pp. 4297–4304, 2001.

[189] D. G. Kaskaoutis, H. D. Kambezidis, P. T. Nastos, and P. G. Kosmopoulos, "Study on an intense dust storm over Greece," *Atmospheric Environment*, vol. 42, no. 29, pp. 6884–6896, 2008.

[190] V. Matthias, D. Balis, J. Bösenberg et al., "Vertical aerosol distribution over Europe: statistical analysis of Raman lidar data from 10 European Aerosol Research Lidar Network (EARLINET) stations," *Journal of Geophysical Research*, vol. 109, p. D18201, 2004.

[191] C. Böckmann, U. Wandinger, A. Ansmann et al., "Aerosol lidar intercomparison in the framework of the EARLINET project. 2. Aerosol backscatter algorithms," *Applied Optics*, vol. 43, no. 4, pp. 977–989, 2004.

[192] V. Matthais, J. Bösenberg, V. Freudenthaler et al. et al., "Aerosol lidar intercomparison in the framework of the EARLINET project. 1. Instruments," *Applied Optics*, vol. 43, no. 4, pp. 961–976, 2004.

[193] G. Pappalardo, A. Amodeo, M. Pandolfi et al., "Aerosol lidar intercomparison in the framework of the EARLINET project. 3. Raman lidar algorithm for aerosol extinction, backscatter, and lidar ratio," *Applied Optics*, vol. 43, no. 28, pp. 5370–5385, 2004.

[194] D. Müller, B. Heinold, M. Tesche et al., "EARLINET observations of the 14–22-May long-range dust transport event during SAMUM 2006: validation of results from dust transport modelling," *Tellus B*, vol. 61, no. 1, pp. 325–339, 2009.

[195] U. Wandinger, A. Hiebsch, I. Mattis, G. Pappalardo, L. Mona, and F. Madonna, "Aerosols and clouds: long-term database from spaceborne lidar measurements," Final Report, 2011.

[196] M. Hess, P. Koepke, and I. Schult, "Optical properties of aerosols and clouds: the software package OPAC," *Bulletin of the American Meteorological Society*, vol. 79, no. 5, pp. 831–844, 1998.

[197] D. S. Balis, V. Amiridis, S. Nickovic, A. Papayannis, and C. Zerefos, "Optical properties of Saharan dust layers as detected by a Raman lidar at Thessaloniki, Greece," *Geophysical Research Letters*, vol. 31, p. L13104, 2004.

[198] G. Pisani, A. Boselli, N. Spinelli, and X. Wang, "Characterization of Saharan dust layers over Naples (Italy) during 2000–2003 EARLINET project," *Atmospheric Research*, vol. 102, no. 3, pp. 286–299, 2011.

[199] S.-H. Wang, S.-C. Tsay, N.-H. Lin et al., "First detailed observations of long-range transported dust over the Northern South China Sea," *Atmospheric Environment*, vol. 45, no. 27, pp. 4804–4808, 2011.

[200] B. Tatarov, D. Müller, Y. M. Noh et al., "Record heavy mineral dust outbreaks over Korea in 2010: two cases observed with multiwavelength aerosol/depolarization/Raman-Quartz lidar," *Geophysical Research Letters*, vol. 39, p. L14801.

[201] Y. Chun and J. Y. Lim, "The recent characteristics of Asian dust and haze events in Seoul, Korea," *Meteorology and Atmospheric Physics*, vol. 87, no. 1–3, pp. 143–152, 2004.

[202] Y. M. Noh, D. Müller, I. Mattis, H. Lee, and Y. J. Kim, "Vertically resolved light-absorption characteristics and the influence of relative humidity on particle properties: multiwavelength Raman lidar observations of East Asian aerosol types over Korea," *Journal of Geophysical Research*, vol. 116, p. D06206, 2011.

[203] K. W. Kim, Z. He, and Y. J. Kim, "Physicochemical characteristics and radiative properties of Asian dust particles observed at Kwangju, Korea, during the 2001 ACE-Asia intensive observation period," *Journal of Geophysical Research*, vol. 109, p. D19S02, 2004.

[204] T. F. Eck, B. N. Holben, O. Dubovik et al., "Columnar aerosol optical properties at AERONET sites in central Eastern Asia and aerosol transport to the tropical mid-Pacific," *Journal of Geophysical Research*, vol. 110, p. D06202, 2005.

[205] N. Sugimoto and C. H. Lee, "Characteristics of dust aerosols inferred from lidar depolarization measurements at two wavelengths," *Applied Optics*, vol. 45, no. 28, pp. 7468–7474, 2006.

[206] Z. Liu, N. Sugimoto, and T. Murayama, "Extinction-to-backscatter ratio of Asian dust observed with high-spectral-resolution lidar and Raman lidar," *Applied Optics*, vol. 41, no. 15, pp. 2760–2767, 2002.

[207] T. Murayama, D. Müller, K. Wada, A. Shimizu, M. Sekiguchi, and T. Tsukamoto, "Characterization of Asian dust and Siberian smoke with multi-wavelength Raman lidar over Tokyo, Japan in Spring 2003," *Geophysical Research Letters*, vol. 31, p. L23103, 2004.

[208] S. A. Young and M. A. Vaughan, "The retrieval of profiles of particulate extinction from cloud-aerosol lidar infrared pathfinder satellite observations (CALIPSO) data: algorithm description," *Journal of Atmospheric and Oceanic Technology*, vol. 26, no. 6, pp. 1105–1119, 2009.

[209] Y. Hu, D. Winker, M. Vaughan et al., "CALIPSO/CALIOP cloud phase discrimination algorithm," *Journal of Atmospheric and Oceanic Technology*, vol. 26, no. 11, pp. 2293–2309, 2009.

[210] Z. Liu, D. Winker, A. Omar et al., "Effective lidar ratios of dense dust layers over North Africa derived from the CALIOP measurements," *Journal of Quantitative Spectroscopy and Radiative Transfer*, vol. 112, no. 2, pp. 204–213, 2011.

[211] G. Pappalardo, U. Wandinger, L. Mona et al., "EARLINET correlative measurements for CALIPSO: first intercomparison results," *Journal of Geophysical Research*, vol. 115, p. D00H19, 2010.

[212] A. H. Omar, J. G. Won, D. M. Winker, S. C. Yoon, O. Dubovik, and M. P. McCormick, "Development of global aerosol models using cluster analysis of Aerosol Robotic Network (AERONET) measurements," *Journal of Geophysical Research*, vol. 110, p. D10S14, 2005.

[213] D. Winker, "Accounting for multiple scattering in retrievals from space lidar," in *Proceedings of the 12th International Workshop on Lidar Multiple Scattering Experiments*, vol. 5059 of *Proceedings of SPIE*, pp. 128–139, September 2002.

[214] D. M. Winker, M. A. Vaughan, A. H. Omar et al., "Overview of the CALIPSO mission and CALIOP data processing algorithms," *Journal of Atmospheric and Oceanic Technology*, vol. 26, no. 11, pp. 2310–2323, 2009.

[215] U. Wandinger, M. Tesche, P. Seifert, A. Ansmann, D. Müller, and D. Althausen, "Size matters: influence of multiple scattering on CALIPSO light-extinction profiling in desert dust," *Geophysical Research Letters*, vol. 37, no. 10, p. L10801, 2010.

[216] L. Mona, G. Pappalardo, A. Amodeo et al., "One year of CNR-IMAA multi-wavelength Raman lidar measurements in correspondence of CALIPSO overpass: level 1 products comparison," *Atmospheric Chemistry and Physics*, vol. 9, pp. 8429–8468, 2009.

[217] R. E. Mamouri, V. Amiridis, A. Papayannis, E. Giannakaki, G. Tsaknakis, and D. Balis, "Validation of CALIPSO space-borne derived attenuated backscatter coefficient profiles using a ground-based lidar in Athens, Greece," *Atmospheric Measurement Techniques*, vol. 2, no. 2, pp. 513–522, 2009.

[218] S. Generoso, I. Bey, M. Labonne, and F.-M. Bréon, "Aerosol vertical distribution in dust outflow over the Atlantic: comparisons between GEOS-Chem and Cloud-Aerosol Lidar and Infrared Pathfinder Satellite Observation (CALIPSO)," *Journal of Geophysical Research*, vol. 113, p. D24209, 2008.

[219] I. Uno, K. Yumimoto, A. Shimizu et al., "3D structure of Asian dust transport revealed by CALIPSO lidar and a 4DVAR dust model," *Geophysical Research Letters*, vol. 35, p. L06803, 2008.

[220] Y. Hara, I. Uno, K. Yumimoto et al., "Summertime taklimakan dust structure," *Geophysical Research Letters*, vol. 35, p. L23801, 2008.

[221] A. Omar, Z. Liu, M. Vaughan et al., "Extinction-to-backscatter ratios of Saharan dust layers derived from in situ measurements and CALIPSO overflights during NAMMA," *Journal of Geophysical Research*, vol. 115, p. D24217, 2010.

[222] C. Textor, M. Schulz, S. Guibert et al., "Analysis and quantification of the diversities of aerosol life cycles within AeroCom," *Atmospheric Chemistry and Physics*, vol. 6, no. 7, pp. 1777–1813, 2006.

[223] V. Matthias, A. Aulinger, J. Bieser et al., "The ash dispersion over Europe during the Eyjafjallajökull eruption—comparison of CMAQ simulations to remote sensing and airborne in-situ observations," *Atmospheric Environment*, vol. 48, pp. 184–194, 2012.

[224] X. Wang, A. Boselli, L. D'Avino et al., "Volcanic dust characterization by EARLINET during Etna's eruptions in 2001–2002," *Atmospheric Environment*, vol. 42, no. 5, pp. 893–905, 2008.

[225] P. Kishcha, P. Alpert, A. Shtivelman et al., "Forecast errors in dust vertical distributions over Rome (Italy): multiple particle size representation and cloud contributions," *Journal of Geophysical Research*, vol. 112, p. D15205, 2007.

[226] V. Amiridis, M. Kafatos, C. Perez et al., "The potential of the synergistic use of passive and active remote sensing measurements for the validation of a regional dust model," *Annales Geophysicae*, vol. 27, no. 8, pp. 3155–3164, 2009.

[227] L. Mona et al., "Quantitative evaluation of DREAM dust modelled profiles with Potenza EARLINET Raman lidar measurements: methodology and first result," submitted to. *Atmospheric Chemistry and Physics*.

[228] K. Yumimoto, I. Uno, N. Sugimoto, A. Shimizu, and S. Satake, "Adjoint inverse modeling of dust emission and

transport over East Asia," *Geophysical Research Letters*, vol. 34, p. L08806, 2007.

[229] K. Yumimoto, I. Uno, N. Sugimoto, A. Shimizu, Z. Liu, and D. M. Winker, "Adjoint inversion modeling of Asian dust emission using lidar observations," *Atmospheric Chemistry and Physics*, vol. 8, no. 11, pp. 2869–2884, 2008.

[230] I. Uno, S. Satake, G. R. Carmichael et al., "Numerical study of Asian dust transport during the Springtime of 2001 simulated with the Chemical Weather Forecasting System (CFORS) model," *Journal of Geophysical Research*, vol. 109, p. D19S24, 2004.

[231] A. Shimizu, N. Sugimoto, I. Matsui, I. Mori, M. Nishikawa, and M. Kido, "Relationship between lidar-derived dust extinction coefficients and mass concentrations in Japan," *Scientific Online Letters on the Atmosphere*, vol. 7, no. 1, pp. 1–4, 2011.

[232] N. Sugimoto, Y. Hara, A. Shimizu, K. Yumimoto, I. Uno, and M. Nishikawa, "Comparison of surface observations and a regional dust transport model assimilated with lidar network data in Asian Dust event of March 29 to April 2, 2007," *Scientific Online Letters on the Atmosphere*, vol. 7, pp. 13–16, 2011.

[233] T. T. Sekiyama, T. Y. Tanaka, A. Shimizu, and T. Miyoshi, "Data assimilation of CALIPSO aerosol observations," *Atmospheric Chemistry and Physics*, vol. 10, no. 1, pp. 39–49, 2010.

[234] T. Nishizawa, N. Sugimoto, I. Matsui, A. Shimizu, and H. Okamoto, "Algorithms to retrieve optical properties of three component aerosols from two-wavelength backscatter and one-wavelength polarization lidar measurements considering nonsphericity of dust," *Journal of Quantitative Spectroscopy and Radiative Transfer*, vol. 112, no. 2, pp. 254–267, 2011.

[235] M. Escudero, X. Querol, A. Ávila, and E. Cuevas, "Origin of the exceedances of the European daily PM limit value in regional background areas of Spain," *Atmospheric Environment*, vol. 41, no. 4, pp. 730–744, 2007.

[236] X. Querol, X. Querol, A. Alastuey et al., "Methodology for the identification of natural African dust episodes in PM_{10} and $PM_{2.5}$, and justification with regards to the exceedances of the PM_{10} daily limit value," Ministry of the Environment of Spain, 2009, http://www.idaea.csic.es/attachments/103_Methodology%20for%20natural%20episodes-rev%20final.pdf.

[237] Council of the European Union, "Commission staff working paper establishing guidelines for demonstration and subtraction of exceedances attributable to natural sources under the Directive 2008/50/EC on ambient air quality and cleaner air for Europe," 2011.

[238] A. Boselli, R. Caggiano, C. Cornacchia et al., "Multiyear sunphotometer measurements for aerosol characterization in a Central Mediterranean site," *Atmospheric Research*, vol. 104, pp. 98–110, 2012.

[239] G. P. Gobbi, H. Wille, R. Sozzi et al., "The impact of Saharan advections on Rome PM levels and the LIFE+ "DIAPASON" project," in *Proceedings of the 6th International Workshop On Sand/Duststorms And Associated Dustfall*, Athens, Greece, September 2011.

[240] A. Ansmann, M. Tesche, P. Seifert et al., "Ash and fine-mode particle mass profiles from EARLINET-AERONET observations over central Europe after the eruptions of the Eyjafjallajökull volcano in 2010," *Journal of Geophysical Research*, vol. 116, p. D00U02, 2011.

[241] F. Marenco and R. J. Hogan, "Determining the contribution of volcanic ash and boundary layer aerosol in backscatter lidar returns: a three-component atmosphere approach," *Journal of Geophysical Research*, vol. 116, p. D00U06, 2011.

[242] E. Gerasopoulos, P. Kokkalis, V. Amiridis et al., "Dust specific extinction cross-sections over the Eastern Mediterranean using the BSC-DREAM model and sun photometer data: the case of urban environments," *Annales Geophysicae*, vol. 27, no. 7, pp. 2903–2912, 2009.

[243] G. Pappalardo, A. Papayannis, J. Bösenberg et al., "EARLINET coordinated lidar observations of Saharan dust events on continental scale," *PIOP Conference Series: Earth and Environmental Science*, vol. 7, no. 1, Article ID 012002, 2009.